Available online at www.sciencedirect.com
ScienceDirect
International Journal of Mass Spectrometry 260 (2007) 1–19
International Journal of Mass Spectrometry
www.elsevier.com/locate/ijms

Review

Coincidence studies of the bond-forming reactivity and reaction dynamics of molecular dications

Stephen D. Price *

Chemistry Department, University College London, 20 Gordon Street, London WC1H 0AJ, United Kingdom

Received 11 May 2006; received in revised form 22 June 2006; accepted 23 June 2006
Available online 1 August 2006

Abstract

This review article discusses the recent progress in explaining and understanding the gas-phase bimolecular reactions of small molecular dications. The article focuses on dication reactions which involve the formation of new chemical bonds and their study by a new position-sensitive coincidence methodology. A review of previous investigations of the bimolecular chemistry of molecular dications is also presented, followed by a detailed description of the position-sensitive coincidence methodology as applied to bimolecular interactions. The insight gained from these position-sensitive experiments is illustrated by a discussion of the results of studies of the reaction of CF_2^{2+} with H_2O and the reactions of N_2^{2+} with a variety of neutral species. The overall conclusion from these investigations is that the bond-forming reactions of molecular dications frequently proceed via the formation of a collision complex. These transitory intermediates may decay to the observed products by either charge-separation or neutral loss.

Keywords: Dication; Coincidence technique; Reaction dynamics

Contents

1. Introduction

This review presents recent progress in exploring and understanding the gas-phase chemistry of molecular doubly charged ions (dications), concentrating in particular on the reactive chan-

* Tel.: +44 20 7679 4606; fax: +44 20 7679 7463.
E-mail address: s.d.price@ucl.ac.uk.

1387-3806/$ – see front matter © 2006 Elsevier B.V. All rights reserved.
doi:10.1016/j.ijms.2006.06.018

nels that involve the formation of new chemical bonds. The study of the chemistry and physics of molecular dications is a rapidly expanding area as evidenced by recent reviews covering the stability of molecular dications [1], the properties of multiply charged molecules [2], the gas-phase reactivity of doubly charged species [3,4] and the spectroscopy of dications [5,6]. The range of experiments involving polyatomic di-positively charged species has also broadened considerably over the last decade to include, for example, the interactions of molecular dications with surfaces [7], ligated transition metal dications in the gas-phase [8–10], the chemistry of multiply charged cluster ions [11,12] and the chemistry of 1,2 dications in solution [13]. In parallel with these extensions of dicationic chemistry, our understanding of the details of the double photoionization process has also advanced significantly in recent years, due to the development of sophisticated electron–electron coincidence experiments [14–17]. As the properties of molecular dications have been revealed, it has become apparent that these species may well play a role in the chemistry of energized media. For example, molecular dications have recently been proposed as key species in the synthesis of polycyclic aromatic hydrocarbons in the interstellar medium [18] and the chemistry of planetary ionospheres [19–21].

Within the expanding field of dication chemical physics, this article focuses on the insights into the bond-forming reactions of molecular dications provided by position-sensitive coincidence (PSCO) experiments. These experiments provide a powerful probe of the bimolecular reactivity of molecular dications and the dynamics of these chemical processes. By studying in detail the reactivity and reaction mechanisms of small prototypical dications with neutral molecules, these coincidence experiments are helping provide the fundamental models to understand this new branch of ion–neutral chemistry.

1.1. Properties of isolated molecular dications

The first indication of the existence of molecular dications was associated with the pioneering studies of the ionization of gases and mass spectrometry in 1921 [22]. The first unambiguous observation of a molecular dication (CO^{2+}) was reported 1930 and the first measurement of the double-ionization energies of N_2 and CO was performed in 1931 [23,24]. However, it was not until the 1970s that the application of modern experimental techniques began to reveal the detailed properties of molecular dications, which are highly energized species. Information on the electronic structure of prototypical dications ($N_2{}^{2+}$ and NO^{2+}) was first obtained from the resolved emission spectra of ions generated in discharges [25–27]. Later, rotationally resolved adsorption spectra for $N_2{}^{2+}$ [28–32] and HCl^{2+} [33] were obtained by employing laser predissociation spectroscopy. As recently noted and discussed [5], resolved optical spectra have only been detected for a very few small molecular dications and more general experimental techniques such as Auger spectroscopy [34], double-charge-transfer spectroscopy [35], translational energy spectroscopy [36], charge stripping [37,38] and ion–ion coincidence methods [39] were used to probe the electronic structure of a wider range of dications. Such experiments were complimented by the application of *ab initio* computational methods to generate potential energy surfaces for the low lying electronic states of several small dications [40,41].

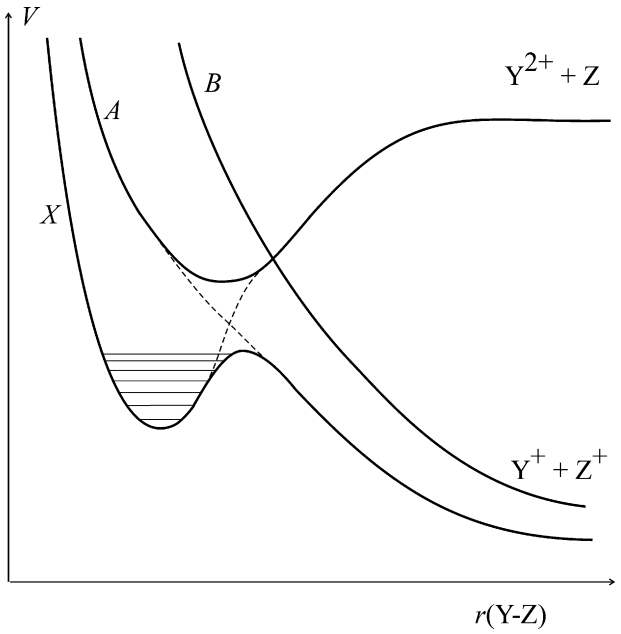

Fig. 1. Schematic potential energy curves for a diatomic dication YZ^{2+}.

With regard to the electronic structure of molecular dications, the research effort reviewed above revealed the general characteristics illustrated in Fig. 1. As Fig. 1 shows, many dication electronic states are purely dissociative (state B, Fig. 1) and the population of such dissociative states results in a translationally energetic pair of monocations. Such fragment monocations often share between them kinetic energy releases in excess of 5 eV [39]. In addition to such dissociative states, many small molecular dications possess longer-lived "metastable" states which exhibit potential energy minima (states X and A, Fig. 1). The origin of the metastability of dication electronic states has been discussed extensively in the literature, where the criteria for the occurrence of thermodynamically stable and metastable states has been considered [1,42]. For small molecular dications composed of light elements, the thermodynamic limit for dissociation of the dication YZ^{2+} into Y^+ and Z^+ commonly lies below both the dissociation limit to Y^{2+} and Z and the dicationic potential energy minimum. Thus, the YZ^{2+} configuration at the potential energy minimum is thermodynamically unstable. However, in a metastable state kinetic stability is conferred on the YZ^{2+} configuration by a potential energy barrier on the pathway to the charge separated products $Y^+ + Z^+$, as illustrated in Fig. 1. Such barriers are often viewed as arising from the avoided crossing of the diabatic potential surfaces correlating with the $Y^{2+} + Z$ and $Y^+ + Z^+$ asymptotes. The surface correlating with the dication and neutral limit is attractive at large interspecies separation, whilst the surface converging on the pair of monocations is purely repulsive. Thus, as illustrated in Fig. 1, the avoided crossing between these potentials results in at least one potential energy surface possessing a minima separated from the $Y^+ + Z^+$ asymptote by a potential energy barrier. Such dicationic

potential energy wells can be several electron volts in depth and support a large number of vibrational levels [41].

Of course, the simple model represented in Fig. 1 is purely two-dimensional, and for polyatomic dications we will have the additional complexity of a multi-dimensional potential energy surface. However, where such potential energy surfaces have been investigated computationally, the essential features illustrated in Fig. 1 are still present [40]. Metastable dication states still exist, trapped behind barriers which can again be viewed as arising from avoided crossings. Of course, the multi-dimensionality of the potential energy surfaces of polyatomic dications allows for additional complexity, for example, the competitive dissociation of individual electronic states to two or more asymptotes [40].

One would expect the lifetimes of dications in metastable states to depend strongly on their vibrational energy content. Dications in high-lying vibrational levels should be able to tunnel rapidly through the barrier to charge-separating dissociation, where as dications with lower vibrational energy content will be trapped behind this barrier. In fact, due to the $1/r$ dependence of its outer wall, the barrier to charge-separating dissociation broadens rapidly with decreasing vibrational energy content. Thus, the tunnelling lifetimes of dicationic metastable vibrational states will increase dramatically with decreasing vibrational energy. However, it appears that the principal decay pathway for the majority of metastable dications is via a curve crossing, if available, to a dissociative electronic state [5,31,32,43,44]. For metastable dication states which are not the ground state, the probability of a predissociative curve crossing onto a dissociative potential correlating with a lower dissociation asymptote is significant. Thus, for excited metastable states the lifetime of an individual vibrational level will usually depend principally on the coupling of that level to the available dissociation continua via predissociative interactions. Given the above analysis, many dicationic metastable vibrational levels should live for a sufficient length of time to encounter other neutral molecules and experience the bimolecular interactions that are the focus of this article. These deductions are confirmed by the available experimental evidence, which shows that many small molecular dications in metastable states possess lifetimes of at least the order of microseconds and sometimes on the order of seconds [45–47].

In the last 15 years the development of sophisticated experimental techniques, such as Doppler-free kinetic energy release spectroscopy [48,49] and photoelectron–photoelectron coincidence spectroscopy (PEPECO) [50–57], has revealed highly detailed information on the vibronic structure of small molecular dications which can be formed by non-dissociative double ionization of stable molecules, such as N_2^{2+}. However, despite this experimental progress, the electronic structures of dications, such as CF_2^{2+}, which cannot be formed by non-dissociative double ionization of a stable molecule, remain much harder to probe at a vibrationally resolved level.

As described above, the majority of dicationic electronic states are dissociative and the dynamics of these unimolecular dissociation reactions have been probed, at a remarkable depth, by a variety of multi-particle coincidence techniques. Particularly relevant to the bimolecular experiments which are the focus of this review article are the PSCO experiments of Eland et al., which study the dissociation reactions of dications [58–60]. When applied to the these processes, for example reaction (1), the PSCO technique involves the coincident detection of the pair of product monocations using a time-of-flight (TOF) mass spectrometer (MS) equipped with a position-sensitive detector:

$$SO_2^{2+} \rightarrow O^+ + S^+ + O \quad (1)$$

From these PSCO signals the nascent velocities of the fragment ions can be determined. The real power of the PSCO technique is realized for the study of dissociation reactions, such as reaction (1), which produce a neutral species in addition to the pair of product monocations; so-called "three-body" reactions. For such three-body reactions the PSCO data allows the velocity of the third (neutral) fragment to be derived from the experimentally determined velocities of the product monocations, completely characterizing the kinematics of the dissociative process.

1.2. Formation of molecular dications

This review deals with the bimolecular bond-forming reactivity of molecular dications with neutral molecules. Given this objective, it is also appropriate to discuss briefly the formation of molecular dications. Typical double-ionization energies usually lie above 20 eV, and for small molecules are often above 30 eV. In this regard, Tsai and Eland proposed a useful empirical rule that the double-ionization energy is usually approximately 2.4 times the single ionization energy [61].

As discussed above, many electronic states of molecular dications are purely dissociative, fragmenting to yield a pair of product monocations or, more rarely for small molecules, a daughter dication and an associated neutral [62–65]. In addition to this dissociative double ionization, long-lived molecular dications can be generated for many small molecules by population of a metastable dicationic electronic state from the neutral molecule. However, metastable dicationic states are not accessible from the neutral for all molecules, often due to unfavourable Franck–Condon factors. For example, long-lived electronic states of CH_4^{2+} cannot be populated from the neutral molecule in significant abundance, whilst H_2O^{2+} seems to have no stable or metastable configuration [66]. Dications which cannot be readily generated from the relevant neutral molecule can, in some cases, be generated via ionization of the relevant monocation using, for example, charge stripping collisions [37,67–70]:

$$SiF^+ + M \rightarrow SiF^{2+} + e^- + M \quad (2)$$

In general, experiments to study the reactivity of molecular dications have generated the relevant reactants using either photoionization or electron ionization. The phenomenon of double photoionization, using either synchrotron radiation or VUV light, has been extensively investigated experimentally as the concerted process provides a fundamental example of a "three-body problem" as the pair of electrons leave the field of the

dication [14,71–73]:

$$M + h\nu \rightarrow M^{2+} + e_1^- + e_2^- \quad (3)$$

However, a variety of experiments have shown that, even close to the double photoionization threshold, dications can be formed by both concerted two-electron ejection [reaction (3)] and a stepwise mechanism [reactions (4) and (5)] involving the initial formation of an excited monocation:

$$M + h\nu \rightarrow M^{+*} + e_1^- \quad (4)$$

$$M^{+*} \rightarrow M^{2+} + e_2^- \quad (5)$$

A conclusion from electron–electron coincidence spectroscopy is that close to the double-ionization threshold for small molecules, double photoionization is often predominantly via the concerted (direct) mechanism, whilst in atoms the indirect process dominates [66]. A variant on this stepwise double-ionization pathway involves the dissociation of the excited monocation intermediate (M^{+*} in Eq. (4)) to give a monocation together with an electronically excited neutral. The subsequent autoionization of this neutral species [reaction (6)] provides a mechanism for the formation of monocation pairs below the double-ionization potential [51,74–77]:

$$M + h\nu \rightarrow M^{+*} + e_1^-$$

$$M^{+*} \rightarrow M_A^+ + M_B^* \text{ followed by } \quad M_B^* \rightarrow M_B^+ + e_2^- \quad (6)$$

For ion beam experiments, the generation of molecular dications via electron ionization offers some experimental advantages over photoionization, as large fluxes of incident electrons can be generated and the energies of these incident electrons can be readily tuned to the optimum value for dication formation. Recent experiments have shown that the contribution of dissociative multiple ionization to the ion yield following electron–molecule collisions has been significantly underestimated in many determinations of partial electron ionization cross-sections [64,65,78–84]. This underestimation arose as many of the energetic fragment ions from the unimolecular dissociation of multiply charged ions were lost in the conventional mass spectrometers used to quantify ion yields. However, the yields of long-lived parent multiply charged ions, for example CO_2^{2+} from the ionization of CO_2, should be accurately determined in such experiments as the dication will have a low initial translational energy. Typically, measurements of partial ionization cross-sections indicate that the formation of long-lived "parent" doubly charged ions can constitute a few percent of the ion yield for small molecules at electron energies of 70 eV and that the maximum yield of such dications occurs at electron energies between 100 and 200 eV [65,85]. The yields of multiply charged ions generated by dissociative multiple ionization, for example CF_2^{2+} from ionization of CF_4, may perhaps have been underestimated in earlier determinations of partial ionization cross-sections due to their potentially significant translational energy, particularly if they are formed via dissociative triple ionization.

In only a few experiments has the "state selective" preparation of molecular dications for ion beam experiments been attempted [86]. In such experiments the principle problem is to generate a usable flux of dications under the constraints imposed by state selection. However, the short-lived nature of the majority of dication electronic states does mean that only long-lived vibronic levels of metastable electronic states will survive long enough to travel from the source region to interact with a neutral molecule. One could therefore argue that the nature of dicationic potential energy surfaces bestows on dication beams an intrinsic level of state selectivity.

In the PSCO experiments described below molecular dications are generated by electron ionization and allowed to interact with neutral molecules. Before describing the PSCO experiment in detail, a brief overview of earlier studies of the bond-forming reactivity of molecular dications will be presented.

1.3. Bimolecular interactions of molecular dications

The first studies of the interactions of molecular dications with other atoms and molecules were carried out at high collision energies (keV) in adapted conventional mass spectrometers. These studies, of dications such as $C_6H_6^{2+}$, CH_3I^{2+}, CO^{2+} and CS_2^{2+}, revealed a reactivity dominated by single-electron-transfer reactions and collision-induced dissociation [87–98]:

$$C_6H_6^{2+} + Ar \rightarrow C_6H_6^+ + Ar^+ \quad (7)$$

$$C_6H_6^{2+} + Ar \rightarrow C_5H_3^+ + CH_3 + Ar^+ \quad (8)$$

$$CO^{2+} + He \rightarrow C^+ + O^+ + He \quad (9)$$

Dicationic single-electron-transfer reactions are commonly subdivided into two categories. In non-dissociative electron-transfer (NDET) reactions, such as Eq. (7), the transfer of the electron from the neutral species to the dication generates product monocations in stable electronic states. Conversely, dissociative (DET) electron-transfer reactions, such as Eq. (8), result in the formation of neutral species in addition to a pair of monocations. As will be discussed in more detail below, DET reactions are commonly considered as sequential processes. In this sequential mechanism, the electron transfer between the reactants forms one, or both, of the primary monocations in a dissociative electronic state (Eq. (10)). Later, often when the product ions are well-separated, the unstable monocation fragments to give the detected products (Eq. (11)):

$$C_6H_6^{2+} + Ar \rightarrow C_6H_6^{+*} + Ar^+ \quad (10)$$

$$C_6H_6^{+*} \rightarrow C_5H_3^+ + CH_3 \quad (11)$$

As discussed briefly below, recent experimental results have questioned the ubiquity of this sequential DET mechanism.

In the high collision energy regime, energy transfer processes sometimes compete with electron-transfer reactions. Excitation of the dication in the collision with the neutral target can result in the population of dissociative dicationic states [92,99,100]. These states can dissociate, as expected given the studies of the behaviour of isolated dications, by charge-separation to form a pair of monocations (Eq. (9)). It is still unclear as to whether the

excitation by the collision is predominantly vibrational, populating short-lived levels near the top of the metastable well, or vibronic, populating excited dissociative electronic states. In addition, and in contrast to the commonly observed behaviour of small isolated molecular dications, collisional excitation of dicationic species can also result in the loss of neutral species to form a daughter dication [101–103]. Such neutral loss decay channels are well documented for the unimolecular decay of large dications [62,63] but are much less frequently observed as relaxation processes for small dications [64,65].

In the late 1980s and 1990s purpose built experiments extended investigations of dicationic bimolecular reactivity to collision energies below 100 eV. These experiments commonly involved the rare gases as collision partners and again revealed product channels dominated by electron transfer and collision-induced dissociation [3,94,99,100,104–107]. As has been described before in the literature, in this collision energy regime the electron-transfer reactivity was usually satisfactorily rationalized using models based on Landau-Zener theory [3,4,108].

Despite the observed propensity for the interactions of molecular dications with neutrals to result in electron transfer, experiments in 1989, involving collisions at thermal collision energies in a drift tube, showed that molecular dications can also exhibit "bond-forming" chemistry [109]:

$$O_2^{2+} + NO \rightarrow NO_2^{+} + O^{+} \quad (12)$$

Indeed, at a similar date the bond-forming chemistry of bare atomic dications was also first observed in the gas phase [110–112]. However, it was not until 1994 that analogous bond-forming reactivity, involving a variety of dications such as CF_2^{2+}, CO_2^{2+} and SF_3^{2+}, was observed in crossed-beam experiments [113]. For example

$$CF_2^{2+} + D_2 \rightarrow DCF_2^{+} + D^{+} \quad (13)$$

Following these initial observations, the bond-forming reactivity of small molecular dications has been studied by conventional crossed-beam experiments [114–123], angularly resolved cross-beam experiments [3,124–127] and guided ion beam experiments [18,86,128–131]. These experiments have revealed several general classes of bond-forming reactions. One such class of reactivity, first observed for atomic dications but now also observed for molecular species, is the generation of dicationic products [115,129]:

$$CO^{2+} + Ar \rightarrow ArC^{2+} + O \quad (14)$$

Reactions such as (14) often have markedly smaller cross-sections than the competing electron-transfer reactions which occur in the same collision systems. The second major class of bond-forming reaction, and the class on which this review will concentrate, is exemplified by reaction (13) where the dication–neutral interaction results in the formation of a pair of product monocations [113,122,123,126,127]. This class of bond-forming reactions often generate neutral species in addition to the pair of monocations:

$$CF_3^{2+} + D_2 \rightarrow DCF_2^{+} + D^{+} + F \quad (15)$$

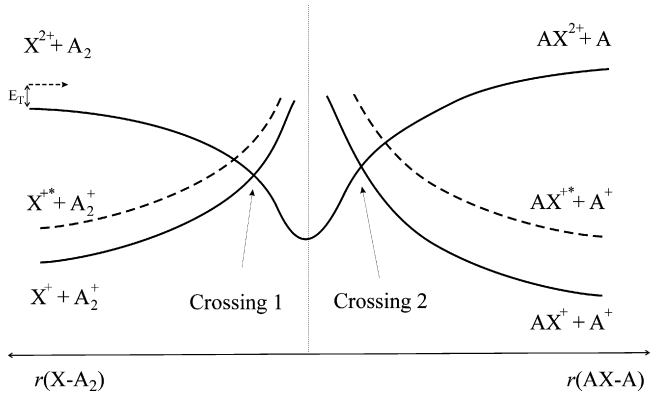

Fig. 2. Schematic potential energy surface for a bond-forming reaction of a molecular dication, as proposed in Ref. [126]. The figure shows that if the collision system can pass though the curve crossings (crossing 1) in the entrance channel, which lead to simple electron transfer, the dication and neutral can form a collision complex. This collision complex can then rearrange its connectivity and dissociate to form species with new chemical bonds. If the separating products undergo electron transfer in the exit channel (crossing 2) a pair of monocations will be formed.

It is important to appreciate that in a conventional mass-spectrometric experiment the precise details of these dication chemical reactions may be difficult to extract. For example, guided ion beam experiments have revealed that NO^+ was produced following interactions of N_2^{2+} with O_2.[1] However, the question of which species are formed together with the NO^+ ions in this chemical reaction then arises. Even in this simple collision system NO^+, O^+ and N^+ are all potential "partner" charged products in the chemical reaction. However, any O^+ ions, which are detected, can also be formed by a dissociative electron-transfer reaction:

$$N_2^{2+} + O_2 \rightarrow N_2^{+} + O^{+} + O \quad (16)$$

Similarly, any N^+ ions detected can also be formed by DET. Thus, a "one-dimensional" mass spectrum cannot determine the precise form of the bond-forming reaction of N_2^{2+} with O_2. Such shortcomings of "one-dimensional" mass-spectrometric techniques for completely characterizing dication reactivity have, in part, stimulated the experimental developments described in this review.

The first investigation of the reaction dynamics of the bond-forming reactions of molecular dications was carried out using an angularly resolved crossed-beam experiment, a powerful technique for studying monocation–molecule reactions [127]. These pioneering experiments stimulated the first general model for the mechanism of dication–neutral chemical reactions [126], a model illustrated in Fig. 2. The model differentiates the reaction co-ordinates for electron transfer and bond-forming processes, the major product channels in these interactions, and elucidates the competition of these different reactive processes. To undergo a bond-forming reaction, the reactants must negotiate a series of curve crossings leading to electron transfer (Fig. 2). If electron transfer does not occur, the reactants can become

[1] R. Thissen and O. Dutuit, unpublished results, 2006

more intimately associated (an encounter complex) and bond formation and breaking can occur. The "chemical" products, with different connectivity from the reactants, can then separate, with the possibility of electron-transfer processes again occurring in this exit channel. The efficiency of this electron transfer in the exit channel governs whether the chemical products are a pair of monocations or a dication and a neutral. The model illustrated in Fig. 2 has been widely used to rationalize the nature and extent of the bond-forming reactivity of molecular dications.

The established techniques for studying monocation–neutral interactions are particularly suited for investigating dication reactions which generate only a pair of singly charged ions, such as reaction (13); so-called "two-body" reactions. For such reactions, due to conservation of momentum, measurements of the kinematics of just one of the ionic products can be used to deduce the kinematics of the undetected ion. For "three-body" reactions, such as reaction (15), a determination of the kinematics of just one of the charged species does not allow the complete kinematics of the reaction to be determined via conservation of momentum, as there are two undetected products. As stated above, many chemical reactions of molecular dications are three-body processes and an experimental technique more directly suited to studying the dynamics of these processes would be highly desirable. Again, such considerations indicated that a new experimental technique was required for more general investigations of dication reactivity.

Despite the potential shortcomings outlined in the above paragraph, during the last decade the application of established experimental techniques for studying ion–molecule reactions have revealed much information concerning the dynamics of dication–neutral chemical reactions. Initial angularly resolved studies of the angular scattering from reaction (13) showed that the heavy product from this two-body chemical reaction (DCF_2^+) was predominantly forward scattered, indicating a predominantly direct reaction mechanism [126,127]. However, the increased large-angle and backward scattering of the DCF_2^+ ion, with respect to the charge-transfer products (e.g. CF_2^+), provided evidence for some "sticky collisions" involving a reaction intermediate. A subsequent angularly resolved investigation of the reaction between CO_2^{2+} with D_2 strongly indicated that the products involving the formation of new chemical bonds (DCO_2^+ and DCO^+) arose via the formation of an intermediate $[D_2CO_2]^{2+}$ [125]. This conclusion was supported by *ab initio* calculations of critical stationary points on the potential energy surface for the reaction [125]. The mechanism revealed by these *ab initio* calculations is illustrated in Fig. 3, for the reaction with H_2, and involves the initial formation of a $[H_2–CO_2]^{2+}$ collision complex, which subsequently undergoes hydrogen atom migration and then charge separates to form the primary products $HCO_2^+ + H^+$. Supporting evidence for the involvement of collision complexes in the reactions of CO_2^{2+} and CF_2^{2+} with $H_2(D_2)$ was provided by studies of the intramolecular isotope effects observed in the reaction of these dications with HD [120,122]. Long and short-lived collision complexes were also recently implicated by the angular distribution of the reactive scattering from the two-body reaction forming $CHDCl^+$ and D^+ from

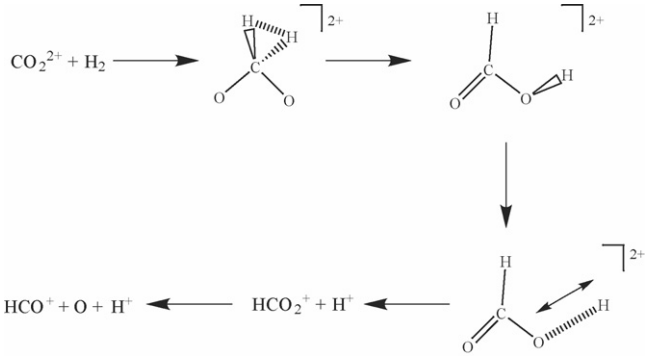

Fig. 3. Proposed mechanism for the formation of HCO^+ and H^+ from the reaction of $CO_2^{2+}$and H_2, derived from *ab initio* calculations of the relevant stationary points on the potential energy surface [125]. Reprinted with permission from Ref. [120]. Copyright 2001, American Institute of Physics.

reactions of $CHCl^{2+}$ with D_2 [124]. Again, the existence of these intermediates was supported by *ab initio* calculations of the relevant stationary points on the potential energy surface. Further indirect evidence for the involvement of collision complexes in the chemical reactions of dications came from an investigation of the formation of ArN^+ and $ArNH^+$ from reactions of Ar^{2+} with NH_3 [116]. In this collision system the collision energy dependence of the relative intensity of the bond-forming products (ArN^+ and $ArNH^+$) could be explained using an *ab initio* reaction pathway that involved initial complexation of the reactants. In addition, the competition between the formation of ArO^{2+} and ArO^+ following collisions of Ar^{2+} with O_2 was also rationalized with a reaction mechanism implicitly involving an ArO_2^{2+} intermediate [132]. More recently, an investigation of the competition between electron transfer and proton transfer in the collisions of CHX^{2+} (X = F, Cl, Br, I) with atoms and molecules concluded that the different lifetimes of encounter complexes determined the reactivity [130].

Given the above overview, it is clear that by the early years of this decade dication–neutral collision complexes had been strongly implicated as potential intermediates in the chemical reactions of molecular dications. However, a new experimental technique to investigate in more detail the dynamics of three-body bimolecular reactions was certainly desirable. Ideally, that technique would also always allow the unambiguous identification of both of the charged species formed in these reactive processes. One method to achieve both these objectives was to apply the PSCO methodology, previously used to study unimolecular reactions of molecular dications, to probe the bimolecular reactivity of these species.

2. Experimental methodology

2.1. Position-sensitive coincidence experiments: the principle

As described above, over the last 20 years the study of both double ionization and the charge-separating unimolecular decay reactions (Eqs. (17) and (18)) of molecular dications have proven a fertile field for the application of a variety of coincidence

methodologies:

$$OCS + h\nu \rightarrow OCS^{2+} + 2e^{-} \quad (17)$$

$$OCS^{2+} \rightarrow O + C^{+} + S^{+} \quad (18)$$

These coincidence experiments have developed in sophistication from simply the detection of the pairs of fragment ions [39] to multi-parameter experiments involving the simultaneous detection of both electrons and ions [60,133]. As also discussed above, considerable insight into the dynamics of the three-body unimolecular dissociation reactions of molecular dications has been achieved by detecting the pairs of fragment ions formed, in coincidence, in a TOF-MS equipped with a detector to determine both the ions' flight times and their arrival positions in the plane perpendicular to the axis of the mass spectrometer. The timing and positional information from such an approach allows the nascent velocity vectors of both of the monocations to be determined. From this pair of ionic velocity vectors, the velocity vector of the undetected neutral fragment in a three-body reaction can be determined by conservation of momentum. Due in large part to the power of this PSCO methodology, the unimolecular dissociation reactions of molecular dications have been characterized at a greater depth than any other class of three-body reactions.

The next section describes how the above PSCO methodology has been implemented to study the bimolecular reactions of molecular dications and is followed by a description of how the resulting timing and positional information is processed to yield the kinematics of each reactive event that is detected.

2.2. Experimental arrangement and data processing

The experimental apparatus for performing PSCO spectroscopy of bimolecular reactions is shown schematically in Fig. 4 and has been previously described in detail in the literature [4,134,135]. As in PSCO experiments to study the unimolecular dissociation reactions of dications, a TOF-MS equipped with a position-sensitive detector is used to collect, in coincidence on an event by event basis, the pairs of singly charged product ions formed by bimolecular dication–neutral reactions.

The reactant dications are generated, via electron ionization of an appropriate precursor gas, in the ion source. These reactant ions, as well as other singly and doubly charged ions, are extracted from the source and pass through a large hemispherical energy analyser with a central radius of 15 cm and an inter-hemisphere gap of 4 cm. This large hemisphere radius is necessary to ensure both good energy resolution ($\Delta E/E = 0.01$) and efficient ion transmission. The analyser is employed to yield an ion beam with an energy spread of approximately 0.3 eV. After leaving the hemispherical energy analyser, the ion beam is pulsed by sweeping the ions backwards and forwards across a small aperture. Using a pulsed ion beam minimizes the spread in the flight times recorded by the TOF-MS by reducing the positional spread of the reactant dications in the mass spectrometer's source region. The constrained velocity spread of the ion beam, resulting from the hemispherical energy analyser, facilitates the formation of spatially well-defined reactant ion pulses.

After exiting the pulsing region, the packets of ions pass through a series of focusing and accelerating lenses, which are tuned to maximize the intensity and optimize the shape of the beam. A commercial velocity filter [136] then selects the

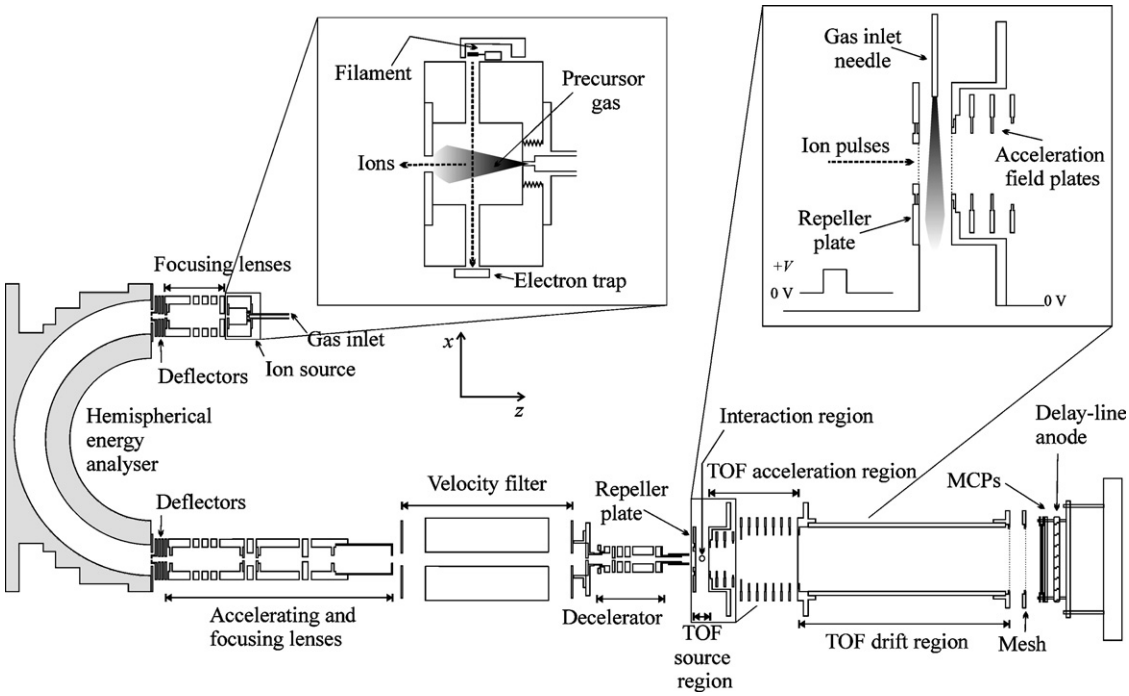

Fig. 4. Schematic of the apparatus employed for the PSCO experiments described in this article. Inset in the figure are enlargements of the ion source and the dication–neutral interaction zone. The latter region is situated in the source region of the TOF-MS.

dications from the packets of ions and the resulting dication pulses are then decelerated to an appropriate collision energy, a few electron volts in the laboratory frame, using a commercial decelerator. Following deceleration, the dication pulses interact with an effusive jet of the neutral gas in the source/reaction region of the TOF-MS and the bimolecular reactions of interest occur. The neutral gas pressure in the reaction region is kept low (below 4×10^{-6} Torr) in order to ensure operation is under single collision conditions [137]. The source region of the TOF-MS is initially maintained in a field-free state to ensure the dication–neutral reactions occur at the required low collision energies. After the reactant ion pulse has almost traversed the source region we record a TOF mass spectrum by applying a positive voltage (50–300 V) to the repeller plate. Mass spectra recorded with a 300 V pulse on the repeller plate result in short enough ionic times of flight to gather the full angular scattering from the dication reactions, despite the considerable kinetic energies of some of the product ions transverse to the axis of the TOF-MS. The longer ionic flight times in mass spectra recorded with lower pulse voltages on the repeller plate result in better energy resolution. However, ions with significant transverse velocities are not detected as they fly beyond the detector radius and thus incomplete angular distributions are recorded. Thus, to gather data with both full angular acceptance and the optimum energy resolution we usually record spectra at both low (50–100 V) and high (300 V) repeller plate voltages.

The TOF-MS is constructed to achieve second-order space focussing [138]. Such focussing minimizes the contribution of the positional spread of the location of the reactive events in the TOF-MS source region to the temporal width of the product ion peaks in the TOF mass spectrum. Note that, as described above, this positional spread is also minimized by employing a pulsed reactant beam. This minimization of the contribution to the temporal widths of the mass spectral peaks is important because, as described below, we evaluate the z (on-axis) velocity component of each ion's laboratory velocity from the deviation of the ion's flight time from the flight time of a zero kinetic energy ion. Thus, to maximize the resolution in the velocities, extraneous contributions to the spread in the ionic times of flight must be minimized.

A few hundred nanoseconds after the voltage pulse is applied to the repeller plate a 'start' pulse is sent to the multi-hit timing electronics. The timing electronics also receive stop signals from the position-sensitive detector at the end of the TOF-MS. The position-sensitive detector is a commercial device in which the electron pulse from a pair of multichannel plates (MCP) impacts on two, perpendicularly wound, wire anodes of known lengths [139,140]. The position of the ionic arrival in the plane of the detector (x, y) can then be derived from the time of arrival of the charge pulse at the end of each anode wire. The charge pulse from the MCP propagates along each wire to its ends and the signals from both the ends of the two wires are passed as stop pulses to the timing circuitry, resulting in four times [$t_{xa}(i)$, $t_{xb}(i)$, $t_{ya}(i)$, $t_{xb}(i)$] for each ion in the pair ($i = 1, 2$). We also record the time of flight of each ion in the pair $t_{\text{expt}}(i)$ by detecting the voltage spike on the MCP supply when an ion is multiplied. Hence, there are five times recorded for each ion arrival, four times from the wire wound anodes and one from the MCP conversion signal; 10 times for each ion pair we detect.

The data processing involved in the PSCO experiment has been previously reported in detail [134,135]. During an experimental run the 10 times associated with each pair event that is detected are simply stored. Thus, the experiment produces a primary dataset which is simply a list of the sets of 10 times characterizing each pair of ions for each of the many thousands of pair events detected during the experimental run. This primary dataset is then processed off-line after the data acquisition has finished. To begin this processing we construct a two-dimensional coincidence ('pairs') spectrum, a histogram of $t_{\text{expt}}(1)$ against $t_{\text{expt}}(2)$ for all the pairs detected. In this pairs spectrum the individual reaction channels appear as distinct peaks allowing immediate identification of both product ions formed in the reaction. We then select, in turn, the groups of events which make up the individual peaks in the pairs spectrum. These subsets of the data can then be processed further to reveal the dynamics of individual reactive channels.

To derive the details of the kinematics for each selected channel we need to determine the x, y and z velocity components for both product ions in the laboratory (LAB) frame and then convert to the centre-of-mass (CM) frame for ease of interpretation. To derive the x and y velocity components of an ion in the LAB frame, $v_x(i)$ and $v_y(i)$, we need to know the position of the ions arrival at the position-sensitive detector. These positions $x(i)$ and $y(i)$, are measured relative to the centre of the detector, and are determined from the difference between the times of arrival of the charge pulse at the ends of each delay line [Eqs. (19) and (20)] together with the calibrated relationship between position and time (1.96 ns mm^{-1}) for the delay lines:

$$x(i) = \frac{t_{xa}(i) - t_{xb}(i)}{1.96} \tag{19}$$

$$y(i) = \frac{t_{ya}(i) - t_{yb}(i)}{1.96} \tag{20}$$

To determine $v_x(i)$ and $v_y(i)$, we also need to know the position (x_0, y_0) of the region where the dication pulses interact with the neutral gas. The co-ordinates x_0 and y_0, are readily determined from the x, y position of the unreacted dication beam at the detector. We also require the total flight time of the ion from the reaction region to the detector. This total flight time is $t_{\text{expt}}(i)$ plus the electronic delay c between the pulsing of the repeller and the start of data collection, where c can be determined by calibration of the mass spectrum. Hence, we have

$$v_x(i) = \frac{x(i) - x_0}{t_{\text{expt}}(i) + c} \tag{21}$$

$$v_y(i) = \frac{y(i) - y_0}{t_{\text{expt}}(i) + c} \tag{22}$$

The z velocity component for each product ion $v_z(i)$ is determined from the deviation of $t_{\text{expt}}(i)$ from the flight time of an ion of the same mass but with zero initial kinetic energy t_0 using Eq. (23). Again, the appropriate value of t_0 can be determined by calibration of the mass spectrum. In Eq. (23), e is the charge on an electron, z the charge number of the ion and F is the electric

field strength in the source region determined via a calibration experiment [134,135]:

$$v_z(i) = -\frac{(t_{\text{expt}}(i) - t_0(i))ezF}{m(i)} \tag{23}$$

Using the above procedure we can derive the LAB frame velocity vectors $v(i) = (v_x, v_y, v_z)$ of both ions ($i = 1, 2$) detected in every pair event. However, the dynamics for the reaction are most clearly revealed when the velocities are presented in the CM frame. To convert the pairs of the LAB velocity vectors $v(i)$ to pairs of velocity vectors $w(i)$ in the CM frame requires the velocity, in the LAB frame, of the CM of the collision system v_c. In general, v_c can be determined from the velocity of the dication in the LAB frame v_{di}, and the mass of the dication and neutral:

$$v_c = \frac{m_{di} v_{di}}{m_{di} + m_{nu}} \tag{24}$$

Here, we assume the dication beam is directed exactly along the z-axis, a reasonable assumption given the quality of our ion beams, and that the velocity of the dication is much larger than that of the effusive neutral molecule, again a good assumption at the collision energies we employ. The velocity of the dication is well defined by the voltages used to allow the ions to pass through the hemispherical energy analyser. The above procedure gives us an average value of v_c for a given experiment. For a two-body reaction, v_c can also be determined from the product velocities for each event detected:

$$v_c = \frac{m(1)v(1) + m(2)v(2)}{m(1) + m(2)} \tag{25}$$

These two methods provide values for v_c in excellent agreement. Once a value of v_c has been determined we can convert the product velocities in the LAB frame to the CM frame:

$$w(i) = v(i) - v_c \tag{26}$$

If the reaction of interest involves the formation of a third, undetected, neutral species its velocity can be now determined via conservation of momentum in the CM frame:

$$w(3) = -\frac{m(1)w(1) + m(2)w(2)}{m(3)} \tag{27}$$

The above procedure results in the CM velocity vectors of the reaction products for each reactive event detected. To reveal the dynamics of the reaction we must then examine the correlations between these velocity vectors.

An initial probe of the correlations between the product velocities is to examine the scattering of these product velocities, in the CM frame, with respect to v_c. This angular scattering is represented using polar histograms, more commonly known as scattering diagrams. A scattering diagram is constructed using the magnitude of $w(i)$ as the radial co-ordinate and the angle φ of $w(i)$ with respect to v_c as the angular co-ordinate. The angle φ is determined from the dot-product of $w(i)$ with v_c. Since $0^\circ \leq \varphi \leq 180^\circ$ the scattering data for one product can be plotted in the upper half of a scattering diagram whilst the data for a second product can be plotted in the lower half, as shown in Fig. 5 for a simple atomic electron-transfer reaction:

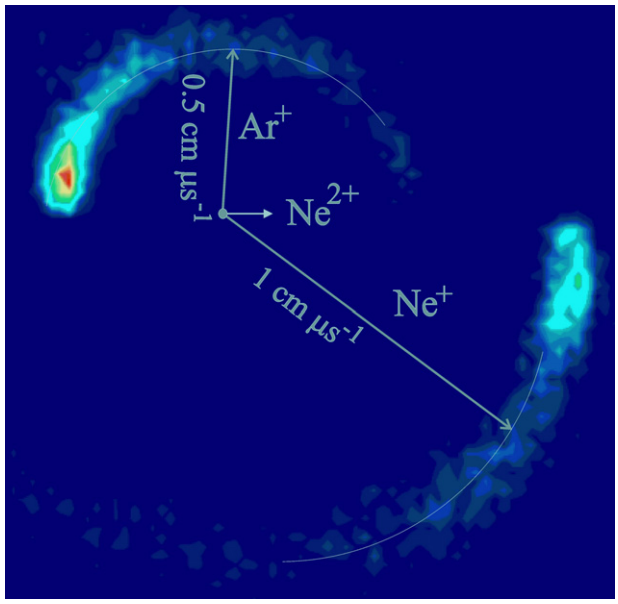

Fig. 5. Scattering diagram showing the velocities of the product ions, Ar^+ and Ne^+ from reaction (28), relative to the velocity of the Ne^{2+} beam at 9.3 eV in the CM frame. As described in the text, the scattering angle for each ion φ lies between 0° and 180°, where $\varphi = 0^\circ$ corresponds to a velocity along the direction of the reactant Ne^+ beam. The data for the Ar^+ product ions are displayed in the upper semicircle of the figure and the data for the Ne^+ ions are displayed in the lower semicircle of the figure. See text for details.

$$Ne^{2+} + Ar \rightarrow Ne^+ + Ar^+ \tag{28}$$

Such simple two-body reactions provide ideal commissioning experiments for the apparatus. The scattering diagram in Fig. 5 clearly shows that forward scattering dominates in this electron-transfer reaction, with the angular distribution of the Ne^+ products strongly peaked in the direction of the velocity of the incident dication. Such characteristic angular scattering has been observed in conventional angular scattering experiments for dication electron-transfer reactions. The physical explanation for the form of this scattering is that electron transfer from the neutral to the dication occurs most efficiently at significant (3–6 Å) interspecies separations, where there is little interaction between the reactants. Thus, the dication just "flies by" the neutral picking up an electron as it passes and the velocities of the product Ne^+ ions are hence strongly aligned with the velocity of the incident Ne^{2+} ions. In principle, the scattering data presented in Fig. 5 could be assembled using a conventional crossed-beam scattering experiment which involves rotating a detector about the scattering centre. However, in such experiments the signals from the ion derived from the neutral species, Ar^+ in this case, are often difficult to access as these ions are slow moving, or even moving in the opposite direction to the incident dications in the laboratory frame. Such detection problems do not occur for the PSCO apparatus. In a conventional experiment, since reaction (28) is a two-body process, the motion and energetics of Ar^+ could be derived from the data for the Ne^+ ion via conservation of momentum. Since the velocities of both product ions

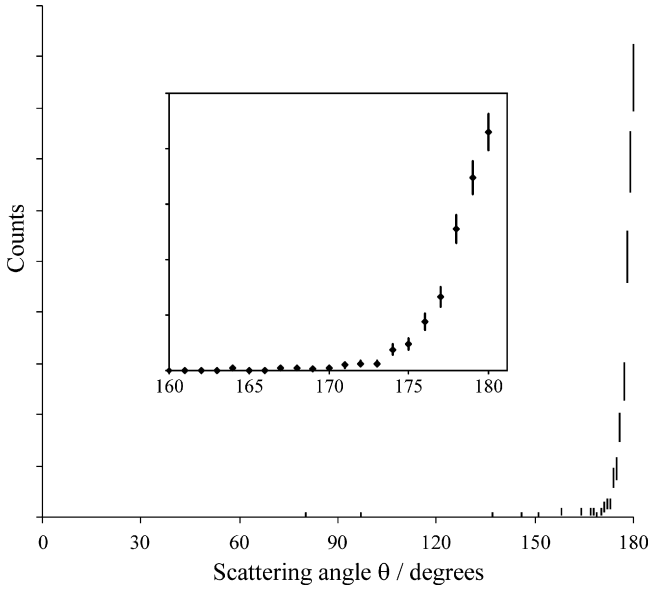

Fig. 6. A histogram of the scattering angle between Ar^+ and He^+ following the electron-transfer reaction of Ar^{2+} with He measured at a CM collision energy of 0.4 eV. The error bars are of length 2σ. Reprinted with permission from Ref. [142]. Copyright 2002, IOP Publishing Ltd.

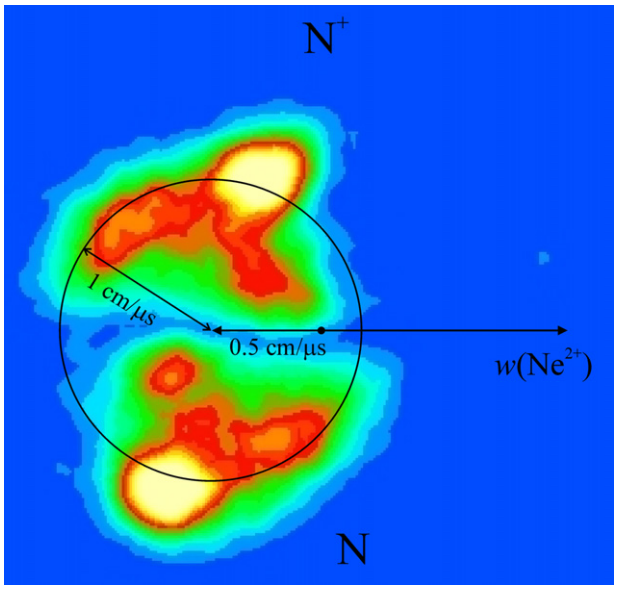

Fig. 7. Internal frame scattering diagram for reaction (30) showing the relationship of the N^+ and N velocity vectors to the velocity of Ne^+ at a CM collision energy of 7.8 eV. The speed in the CM frame of the product ions is the radial co-ordinate and their scattering angle θ (0–180°) with respect to the Ne^+ velocity is the angular co-ordinate. The data for N^+ is shown in the upper semicircle of the figure. This scattering diagram is composed of two reaction channels, one involving complexation and one a sequential mechanism. See Ref. [141] for details.

are determined in the PSCO experiment, we can determine the angle between these velocities for each ion pair we detect. The extraction of this mutual scattering angle θ, which is constrained to 180° by conservation of momentum, provides an excellent test of the operation of the PSCO experiment. A histogram of θ for the electron-transfer reaction between Ar^{2+} and He is shown in Fig. 6. The histogram is peaked at 180°, as it should be, with a half width of 2°, giving a reliable estimate of the angular resolution in the velocities we determine. The above determination of the mutual scattering angle demonstrates one great advantage of the coincidence methodology. Specifically, since the coincidence dataset is effectively just a list of the velocity vectors of the products from each reactive event detected, the dataset can be examined at leisure off-line to search for relevant correlations between the different velocity vectors. As we will see below, different vector correlations may be the most useful dynamical probes in different collision systems.

As discussed above, for a two-body reaction the angle between the velocities of the two ionic products will always be 180°. However, as we will demonstrate below, for three-body reactions the scattering of two of the products relative to the third product, the internal frame scattering, is a very powerful probe of the reaction mechanism [141]. One way of representing the internal frame scattering is in an internal frame scattering diagram which shows the scattering of any two products relative to the third product. Internal frame scattering diagrams are again polar histograms using the magnitude of the velocity of a given ion, for example $w(1)$, as the radial co-ordinate and the angle θ between $w(1)$ and $w(2)$, if ion 2 is to be the reference ion, as the angular co-ordinate. Again, θ can be determined from the dot-product of $w(1)$ with $w(2)$. As with the regular scattering diagram, since $0° \leq \theta \leq 180°$, the internal frame scattering data for ion 1 with respect to ion 2 can be plotted in the upper half of the diagram and the data for ion 3 with respect to ion 2 can be displayed in the lower half, as shown in Fig. 7. Of course, the velocity of any of the three products can be used as the reference velocity for an internal frame scattering diagram.

The PSCO experiment also provides energetic information on the reactive events that are detected. The exothermicity, ΔE, for each reactive event can be expressed in terms of the kinetic energy release of the reaction in the CM frame T and the CM collision energy, E_c:

$$\Delta E = E_{\text{products}} - E_{\text{reactants}} = T - E_c \tag{29}$$

T can be determined from the magnitudes of the CM velocity vectors and E_c can be determined from the dication velocity and the reduced mass of the reactants. Therefore, a histogram of the ΔE values for each reactive event detected can be constructed. This "exothermicity spectrum" may be used to provide information on the states of the reactant dication present in the beam and the product states populated in dication–neutral reactions [134,135,142]. For example, Fig. 8 shows the exothermicity spectrum recorded for another atomic single-electron-transfer reaction, studied for commissioning purposes, between Ar^{2+} and He. The spectrum clearly shows the presence of the ^3P and ^1D electronic states of Ar^{2+} in the dication beam which both react to produce Ar^+ and He^+ in their ground electronic states, as has been observed previously [143]. Again, the coincidence methodology allows us to select from the experimental dataset the events corresponding to the reaction of each of these dication electronic states to probe their angular distributions separately. Such off-line analysis shows that the angular distribution of the

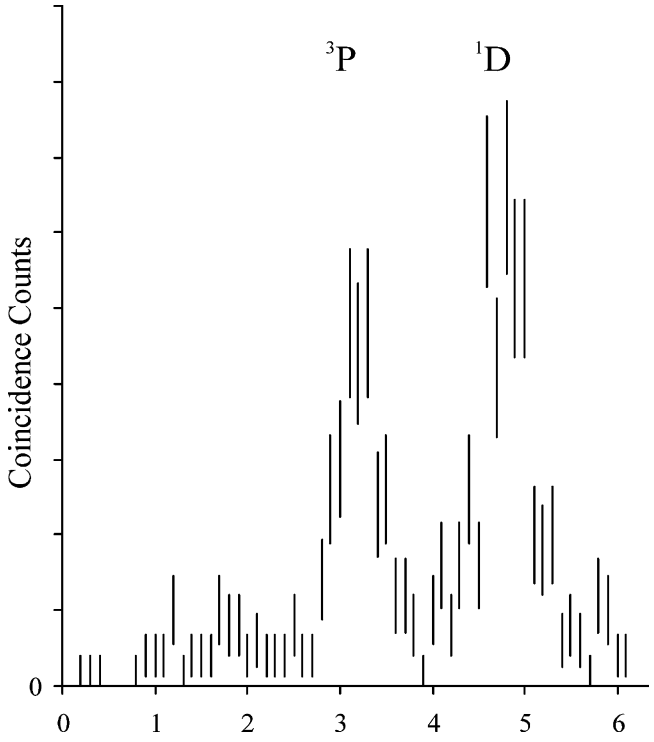

Fig. 8. The exoergicity spectrum for the reaction of Ar^{2+} with He at a CM collision energy of 0.4 eV. The spectrum clearly shows the reaction of the ^{3}P and ^{1}D states of Ar^{2+} to form $Ar^+(^2P)$ and $He^+(^2S)$.

monocation products is different for the reaction of the ^{3}P and ^{1}D states of Ar^{2+} [135,143,144].

Of course, the implementation of the PSCO methodology described above has some shortcomings, several of which will be addressed in a second generation instrument which is currently being designed. The principal shortcoming is the energy resolution in the exothermicity spectrum which, as illustrated in Fig. 8, is approximately 400 meV FWHM. This energy resolution is not sufficient to distinguish the different vibrational transitions involved in the electron-transfer reactions of even diatomic molecular dications, despite the vibrational level spacings in such species being comparable with the current experimental resolution. Significantly better energy resolution is needed to deconvolute the large number of vibronic transitions involved in even a simple molecular electron-transfer reaction if several reactant vibrational states are populated and those states can accept an electron to populate several vibrational states in the product monocation. Representative calculations of Franck–Condon factors indicate that for N_2^{2+} an experimental resolution of approximately 100 meV will be required to reveal the contribution of individual vibrational levels. The energy resolution of the existing PSCO experiment is limited by the positional resolution of the detector, which is determined by the 1 ns resolution of the timing electronics, and by the range of CM collision energies that result from using an effuse thermal jet of the target gas. In a second generation instrument, we plan to employ a molecular beam to restrict the range of collision energies and improved timing electronics to achieve 100 meV energy resolution.

3. Representative results

The PSCO spectra recorded following the interactions of molecular dications with neutrals at low collision energies are remarkably rich, showing many different reactive channels. The most intense of these reactive processes usually involve electron transfer, as illustrated above. The focus of this article is the bond-forming processes which compete with these electron-transfer reactions. However, it is worth noting, in passing, that PSCO studies of dicationic electron-transfer reactions have shown that some of these processes, for example reaction (30), do not always proceed by the expected "sequential" mechanism. In the case of reaction (30), the sequential mechanism would involve an N_2^{+*} ion, formed in the initial electron transfer, dissociating when well-separated from the Ne^+ product ion:

$$Ne^{2+} + N_2 \rightarrow Ne^+ + N^+ + N \quad (30)$$

In fact, PSCO experiments clearly show reaction (30) actually proceeds via two different pathways, one of which involves complexation of the reactants to form a $[NeN_2]^{2+}$ intermediate which then directly dissociates to the atomic products [141].

In contrast to the direct mechanism observed for reaction (30), the PSCO technique has shown that the electron-transfer reactions of CF_3^{2+} follow the expected sequential pathway [142]:

$$CF_3^{2+} + Ar \rightarrow CF_3^{+*} + Ar^+ \quad (31)$$

$$CF_3^{+*} \rightarrow CF_2^+ + F^+ \quad (32)$$

The spectra also show that the excited states of CF_3^+ populated by the primary electron transfer are high-lying vibrational levels of the ground electronic state. Similar conclusions, implicating a sequential mechanism, were drawn from earlier studies of the dissociative electron-transfer reactions of CO_2^{2+} [125].

Returning to the main theme of this article, the dynamics of the bond-forming reactions of molecular dications, there follows a review of recent PSCO results which show the variety of mechanisms observed for these unusual reactive processes.

3.1. $CF_2^{2+} + H_2O$

Of all molecular dications, the dynamics of the low-energy chemical and electron-transfer reactions of CF_2^{2+} have been the subject of the greatest experimental attention. This attention is, in part, a result of the ease of forming useable beams of this dication via dissociative ionization of CF_4. The perfluorination of the target molecule reduces the mass resolution required to generate dication beams uncontaminated by other ions, with a consequent increase in dication beam flux. As discussed above, the reaction of CF_2^{2+} with D_2 was the first low-energy reaction of a molecular dication to be studied by angularly resolved techniques [126,127]. This angularly resolved work, together with studies of intermolecular and intramolecular isotope effects in the CF_2^{2+}/HD(D_2, H_2) collision systems [119,122], hinted that complexation was involved in the reaction mechanism. These experimental conclusions were supported by subsequent theoretical investigations of stationary points on the potential energy surface [119].

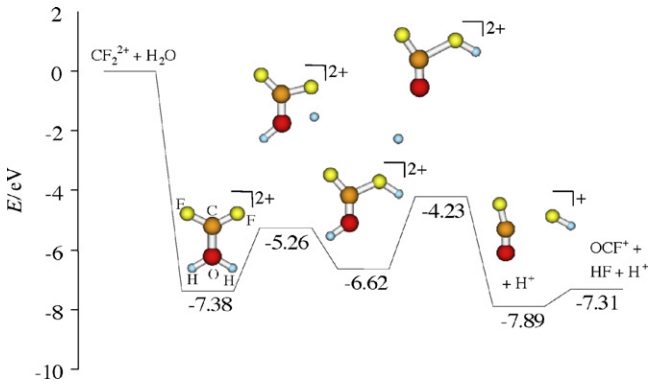

Fig. 9. A schematic representation of the calculated stationary points on the potential energy surface for reaction (33).

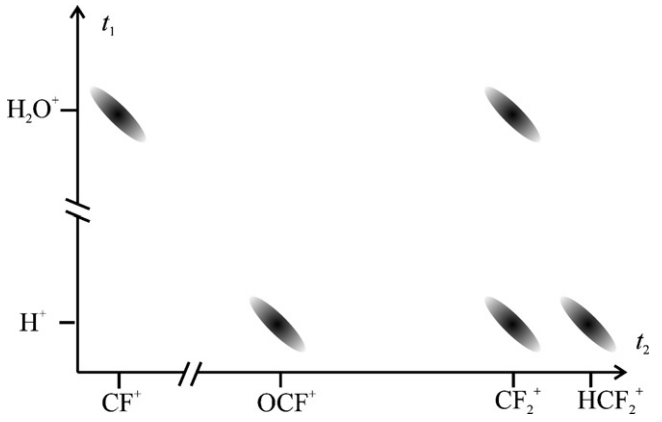

Fig. 10. Schematic PSCO spectrum of the bimolecular reactions observed following collisions of CF_2^{2+} with H_2O at CM energy of 5.6 eV.

Chemical reactions were also observed following the interaction of CF_2^{2+} with H_2O [117]:

$$CF_2^{2+} + H_2O \rightarrow OCF^+ + H^+ + HF \quad (33)$$

The absence of mass-spectrometric signals corresponding to HF^+, F^+ and H_2F^+ from this collision system confirmed that H^+ was the monocation partner of OCF^+. The considerable rearrangement in atomic connectivity in moving from reactants to products in this chemical reaction suggests that complexation is involved in the reaction mechanism.

This observation of such an unusual chemical reaction stimulated an *ab initio* investigation of the key stationary points on the $CF_2^{2+} + H_2O$ potential energy surface [118]. This computational study revealed a broadly analogous mechanism to that discussed above (Fig. 3) for $CO_2^{2+} + H_2(D_2)$. The stationary points on the potential energy surface are illustrated in Fig. 9 which shows that the reaction proceeds initially via formation of a $[H_2O–CF_2]^{2+}$ collision complex which subsequently rearranges to $[HO–C(FH)F]^{2+}$. This dication then undergoes charge-separation to $H^+ + OC(FH)F^+$ with the molecular cation then dissociating to $OCF^+ + HF$. The quantum chemical calculations indicated that the barriers on the above reactive pathway favoured the formation of OCF^+ from the reaction of CF_2^{2+} with H_2O in comparison with D_2O. However, due to the sampling timescale, such an intermolecular isotope effect was not observable in a crossed-beam experiment [118].

Given the above detailed predictions regarding the reaction mechanism, collisions of CF_2^{2+} with H_2O provided an ideal collision system for study by the PSCO technique [145]. As shown schematically in Fig. 10, the PSCO spectra showed clear signals for the previously observed electron-transfer reactions and also for the bond-forming reaction of interest (reaction (33)). The PSCO results unambiguously confirm that H^+ is the monocation that accompanies the formation of OCF^+, as intimated from earlier mass-spectrometric studies [117]. In addition the PSCO spectra also revealed (Fig. 10) weak signals corresponding to a previously unobserved bond-forming process:

$$CF_2^{2+} + H_2O \rightarrow HCF_2^+ + H^+ + O \quad (34)$$

Concentrating first on the reaction forming OCF^+ (reaction (33)), the scattering diagram derived from the PSCO data for the monocationic products is shown in Fig. 11. This scattering diagram reveals that the scattering of H^+ is approximately isotropic with respect to initial CM velocity of the dication. The OCF^+ is also isotropically scattered but with a much lower CM velocity. This symmetrical scattering is that expected for a reaction mechanism which involves the formation of a collision complex which has a lifetime at least comparable with its rotational period. The significant lifetime of the complex means that the velocity vectors of the products of its dissociation are uncorrelated with the initial dication velocity, as clearly shown in Fig. 11.

As described above, the earlier computational investigation of the potential energy surface of this reaction [118] supports this experimental evidence for a collision complex, suggesting a reaction mechanism involving the initial formation of $[H_2O–CF_2]^{2+}$. As described above, the velocity of the neutral species which accompanies the formation of OCF^+ and H^+ can be determined from the monocation velocities recorded for each reactive event. It is important to note that the exothermicity spectra recorded for this reaction clearly indicate that only the stable ground state of HF is populated in this reaction; the reaction is not a four-body process forming H and F atoms. The velocity derived for the HF product is also distributed isotropically very close to the velocity of the centre of mass. From the internal frame scattering diagram for this reaction (Fig. 12) we see that H^+ is quite symmetrically scattered with respect to the velocity of OCF^+, which indicates that the formation of these two ions is separated in time. Fig. 12 also shows the velocity of HF is sharply anticorrelated with that of OCF^+. Such scattering can only result if the collision complex charge separates to form H^+ and $[HO–CF_2]^+$, with the molecular ion subsequently dissociating to HF and OCF^+. Due to the mass difference between H^+ and $[HO–CF_2]^+$ the proton will take with it most of the kinetic energy of the dissociation. Hence, the $[HO–CF_2]^+$ will have a very low velocity in the centre of mass frame. If the $[HO–CF_2]^+$ then lives for a timescale comparable with its rotational period, before dissociating to HF and OCF^+, the H^+ velocity will be uncorrelated with that of OCF^+ as we observe. However, the HF and OCF^+ species formed in this final two-body dissociative process must have velocity vectors which are anticorrelated, as

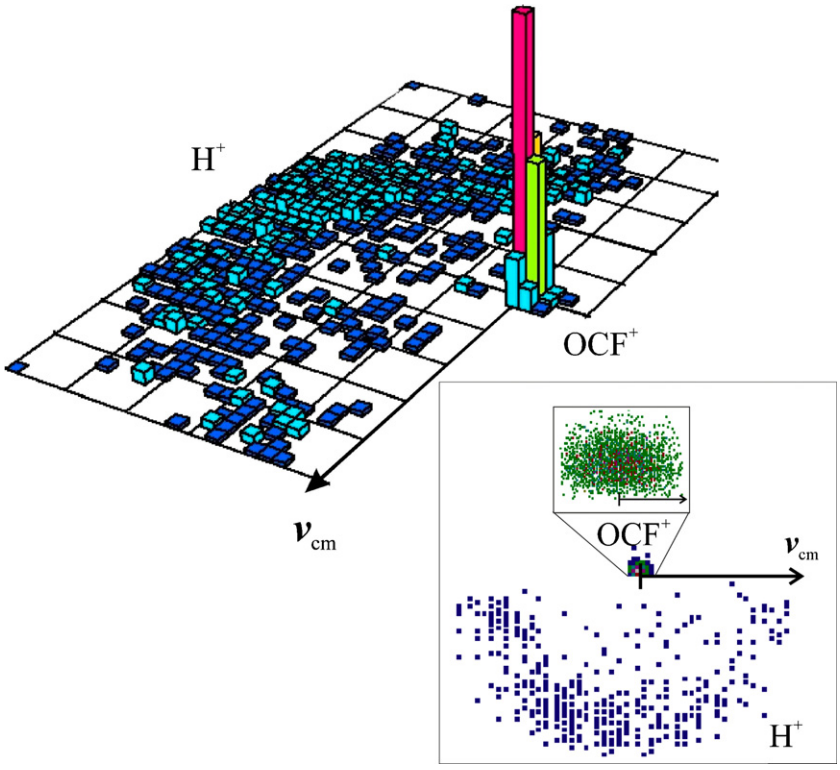

Fig. 11. Two-dimensional and three-dimensional representations of the scattering diagram showing the motion of H^+ and OCF^+ formed in reaction (33) at CM energy of 5.6 eV. In the two-dimensional plot the data for OCF^+ is also plotted on an expanded scale. Reprinted with permission from Ref. [145]. Copyright 2004, American Institute of Physics.

we observe experimentally. The discussion above clearly shows that the PSCO data for the formation of OCF^+ and H^+ is in perfect agreement with the reaction mechanism calculated computationally. The slight asymmetry in the scattering of H^+ with respect to OCF^+ in Fig. 12, can readily be accounted for if the dissociation of $[HO–CF_2]^+$ occurs within the field of the departing proton.

Considering the weaker bond-forming reaction generating HCF_2^+ and H^+, the scattering diagram for this channel shows that H^+ is approximately isotropically scattered, with a large

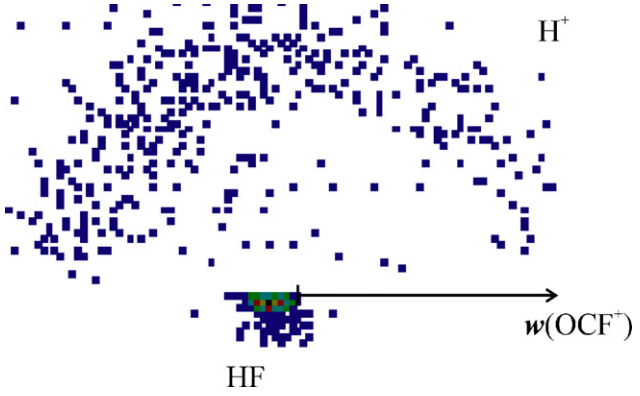

Fig. 12. Internal frame scattering diagram showing the motion of H^+ and HF, formed in reaction (33), relative to OCF^+. The data for H^+ is plotted in the upper half of the figure and the data for HF in the lower half. Reprinted with permission from Ref. [145]. Copyright 2004, American Institute of Physics.

velocity, in the CM frame with respect to the initial dication velocity [145]. In contrast, HCF_2^+ is forward scattered and O is backscattered and both of these heavy species have markedly lower CM velocities than H^+ [145]. The scattering of the H^+ ion again points to the presence of a long-lived species in the reaction pathway. However, the scattering in this channel is significantly different from that involved in the formation of $OCF^+ + H^+ + HF$. Specifically, the molecular ionic product and the neutral are not isotropically scattered in the CM frame, indicating a fundamentally different mechanism is operating in comparison with the formation of $OCF^+ + H^+ + HF$. The forward scattering of the HCF_2^+ with respect to the initial dication velocity is indicative of a "direct" reaction mechanism where the CF_2^{2+} "flies by" the H_2O molecule picking up a hydride ion as it passes, leaving an OH^+ partner ion. As described above, such strong forward scattering is also observed in dicationic electron-transfer reactions where the reactant ion flies past the neutral picking up an electron [3,134]. If the OH^+ partner ion then lives long enough to rotate significantly before decaying to $H^+ + O$, the H^+ ion will be isotropically scattered with respect to the initial velocity of the dication, as we observe. If the OH^+ primary product decays when well-separated from the HCF_2^+ ion, we would expect the H^+ and O atom velocities to be distributed symmetrically about the final OH^+ velocity. Such behaviour has been observed in PSCO data from "slow" dissociative electron-transfer reactions [4]. We can estimate the expected final velocity of the OH^+ intermediate, by conservation of momentum, from the velocity for the HCF_2^+ ion. This velocity is indicated in the internal frame

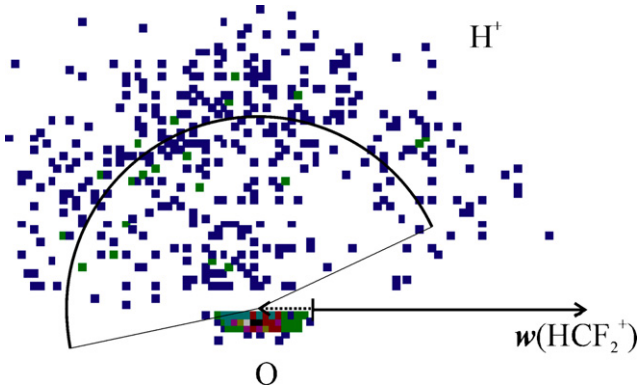

Fig. 13. Internal frame scattering diagram showing the motion of H^+ and O, formed in reaction (34), relative to HCF_2^+. Marked on the figure as a dotted arrow is $w(OH^+)$, the calculated precursor velocity of an OH^+ ion formed together with the HCF_2^+ ion. The arc represents the H^+ velocity formed from the fragmentation of such an ion with an energy release of 4.2 eV. Reprinted with permission from Ref. [145]. Copyright 2004, American Institute of Physics.

scattering diagram for this reaction (Fig. 13) and we see that the O and H^+ velocities are isotropically distributed about this vector, in excellent agreement with the proposed mechanism. Hence, it seems quite clear that the formation of HCF_2^+ and H^+ proceeds via a direct reaction to form HCF_2^+ and OH^{+*}, with the OH^{+*} subsequently dissociating to H^+ and O. Energetic considerations in fact implicate the population of the $c^1\Pi$ state of OH^+ [146], which is known to predissociate with a large energy release, rather than higher lying unbound levels which will dissociate rapidly [147].

3.2. $N_2^{2+} + O_2$

Recent detailed ionospheric modelling has indicated that long-lived electronic states of molecular dications can play a role in the chemistry of planetary ionospheres [19–21]. For example, recent simulations indicate that CO_2^{2+} is involved in the ionospheric chemistry of Mars and N_2^{2+} in the chemistry of the terrestrial ionosphere. As described briefly in Section 1.3, as part of a research programme designed to elucidate the chemistry of N_2^{2+} and other ionospherically important dications, guided ion beam experiments in Paris have shown that NO^+ is formed in collisions of N_2^{2+} with O_2 (see Footnote 1). However, this mass-spectrometric investigation does not reveal the identity of the partner monocation (and perhaps neutral species) that accompany the formation of the NO^+ ion in this collision system. Thus, collisions of N_2^{2+} with O_2 are an ideal system for investigation by the PSCO technique. An additional advantage of the PSCO technique for such an investigation is that isotopically substituted ($^{14}N^{15}N$) molecular nitrogen is not required as the dication precursor. In conventional mass-spectrometric experiments such isotopic substitution is required to allow the molecular dications, at $m/z = 14.5$, to be distinguished from the N^+ ions. In the PSCO experiments, since only dications can generate the pairs of product ions detected, the use of $^{14}N_2$ and a beam of ions at $m/z = 14$ still allows the accumulation of coincidence spectra revealing the reactivity of the N_2^{2+} dications, despite the presence of atomic nitrogen monocations in the beam.

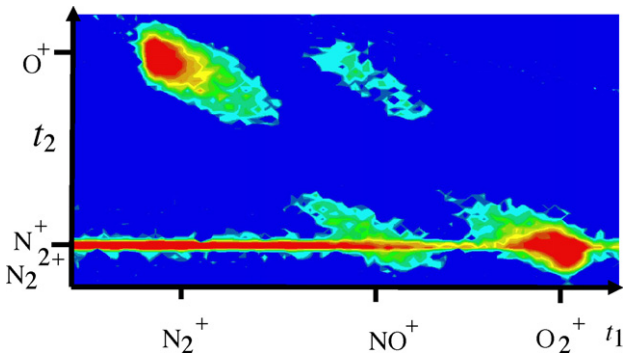

Fig. 14. Section of the coincidence spectrum recorded following collisions of N_2^{2+} with O_2 at 7.1 eV. The spectrum clearly shows the two bond-forming reactions that occur in this collision system [Eqs. (35) and (36)]. The horizontal line in the spectrum, at the time of flight of $m/z = 14$, is due to the contribution of false coincidences involving an unreacted ion. Reprinted with permission from Ref. [148]. Copyright 2005, American Institute of Physics.

The bimolecular reactions between N_2^{2+} and O_2 were studied using the PSCO technique, at a range of CM collision energies between 4 and 12 eV [148]. Five dominant bimolecular reactions were clearly seen in the coincidence (pairs) spectra. A section of a typical coincidence spectrum is presented in Fig. 14. The reactions observed involve both non-dissociative electron transfer and dissociative electron transfer, together with two bond-forming channels [Eqs. (35) and (36), Fig. 14]:

$$N_2^{2+} + O_2 \rightarrow NO^+ + O^+ + N \quad (35)$$

$$N_2^{2+} + O_2 \rightarrow NO^+ + N^+ + O \quad (36)$$

The horizontal line in the portion of the coincidence spectrum displayed in Fig. 14 arises from false coincidences with unreacted ions (principally N^+ ions) in the dication beam. However, the bond-forming channels can be easily distinguished from this false coincidence signal, although the false coincidences must be subtracted before further data processing occurs. After this pre-processing the PSCO intensities reveal that the two bond-forming reactions are equally intense and that the bond-forming events are about five times less frequent than dissociative electron-transfer events.

3.2.1. Formation of $NO^+ + O^+ + N$

The exothermicity spectrum for this reactive channel is broad and unresolved indicating only that the reaction exothermicity is distributed between ~1 and 12 eV with a maximum at approximately 4 eV. As described in the literature, the upper limit of the observed exothermicities corresponds well with the formation of the products in their ground states from the ground $X(^1\Sigma_g^+)$ state of N_2^{2+}. The range of exothermicities observed experimentally is consistent with the formation of NO^+ with a wide range of vibrational excitation [148].

The scattering diagrams derived from the PSCO data for the formation of $NO^+ + O^+ + N$ show that all the products from this channel are predominantly sideways scattered, relative to the velocity of the CM, over a relatively large range of scattering angles [148]. As described above, such scattering is a very strong indication that the products have been formed from the

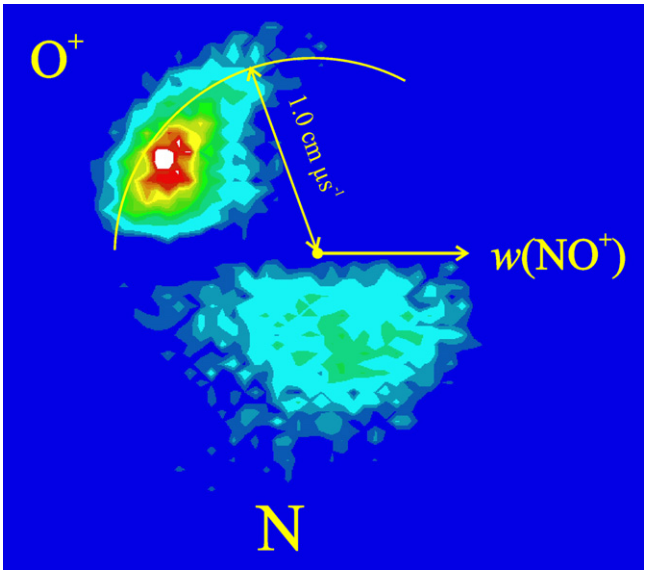

Fig. 15. Internal frame scattering diagram showing the motion of O^+ and N formed in reaction (35), recorded following collisions of N_2^{2+} with O_2 at 7.1 eV, relative to that of NO^+. In this diagram $w(i)$ is the radial co-ordinate and the angle between $w(i)$ and $w(NO^+)$ is the angular co-ordinate. The data for O^+ is plotted in the upper semicircle of the figure and the data for N in the lower semicircle. Reprinted with permission from Ref. [148]. Copyright 2005, American Institute of Physics.

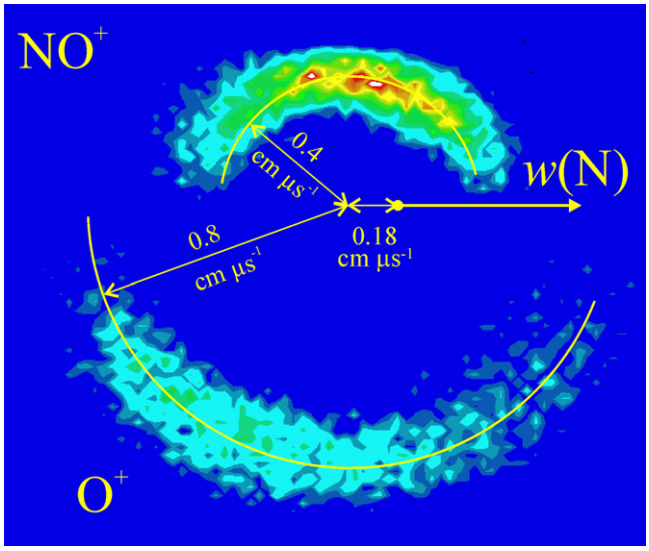

Fig. 16. Internal frame scattering diagram showing the motion of NO^+ and O^+ formed in reaction (35), recorded following collisions of N_2^{2+} with O_2 at 7.1 eV, relative to that of N. In this diagram $w(i)$ is the radial co-ordinate and $\theta(i)$ the angle between $w(i)$ and $w(N)$ is the angular co-ordinate. The data for NO^+ is plotted in the upper semicircle of the figure and the data for O^+ in the lower semicircle. Reprinted with permission from Ref. [148]. Copyright 2005, American Institute of Physics.

break-up of a collision complex, $[N_2O_2]^{2+}$ in this case. The internal frame scattering diagram presented in Fig. 15 shows that there is a marked anti-correlation between the velocities of the charged products NO^+ and O^+. That is, the O^+ ion is scattered strongly in the opposite direction to the NO^+ product. Conversely, Fig. 15 also shows that the velocity of the N atoms is not strongly correlated with either of the velocities of the charged products. Consideration of the possible scattering mechanisms [148] shows that the only reaction pathway compatible with this PSCO data involves a collision complex initially losing a neutral species and the resulting dication later dissociating (37):

$$[N_2O_2]^{2+} \rightarrow NO_2^{2+} + N \rightarrow NO^+ + O^+ + N \quad (37)$$

This reaction mechanism will result in the velocity of the N atom being markedly lower than, and not strongly correlated with, the velocities of either of the charged products. Conversely, the scattering of the charged products will involve them having mutually anticorrelated velocities which are not correlated with the motion of the centre of mass.

Further evidence in favour of the above reaction mechanism, involving initial neutral loss from the collision complex, is provided by consideration of the magnitudes of the velocities of the products. The modal velocity of the N fragment is 0.6 cm μs^{-1}. Thus, by conservation of momentum, the velocity of the NO_2^{2+} ion formed in the initial neutral loss step should be 0.18 cm μs^{-1}. That is, if the "neutral loss" mechanism (37) is operating we would expect the NO_2^{2+} to be moving away from the centre of mass at 0.18 cm μs^{-1} in the opposite direction to the N atom. As shown in Fig. 16 the centres of the isotropic distributions of the charged species are indeed displaced from the velocity of the CM by close to this velocity. When viewed in this displaced frame, as illustrated in Fig. 16, the velocities of the ionic products are consistent with the two-body dissociation of an NO_2^{2+} ion; that is, the magnitudes of the momenta of the NO^+ and the O^+ ions are equal. Indeed, the velocities of the O^+ and NO^+ indicate an average kinetic energy release upon dissociation of 7.8 eV, in agreement with the energy release reported for the dissociation of long-lived NO_2^{2+} ions [149,150].

In the light of the above analysis, the PSCO data clearly indicate that this reactive channel proceeds, as indicated in Eq. (37), via initial neutral loss from a collision complex followed by charge-separation of the resulting NO_2^{2+} dication.

Theoretical support for the existence of a collision complex in the reaction of N_2^{2+} with O_2 comes from quantum chemical calculations which indicate a "tetrahedral" $[N_2O_2]^{2+}$ (C_{2v}) minimum on the singlet potential energy surface [148], a geometry analogous to that predicted for the isoelectronic species N_4 and N_3O^+. This minimum lies 4.8 eV below the reactant asymptote of $N_2^{2+}(^1\Sigma_g^+) + O_2(^3\Sigma_g^-)$ [148]. On the triplet $[N_2O_2]^{2+}$ surface, further quantum chemical calculations reveal a "linear" (C_s) minimum with connectivity N–N–O–O. This "linear" triplet minimum lies 8.2 eV below the $N_2^{2+}(^1\Sigma_g^+) + O_2(^3\Sigma_g^-)$ reactant asymptote [148]. The reactant N_2^{2+} beam certainly contains dications in the $X(^1\Sigma_g^+)$ ground state and probably dications in the $c(^3\Sigma_u^+)$ state. Hence, in principle, both the singlet and triplet complexes are accessible in spin-allowed processes from the ensemble of reactant molecules. Intuitively, given their respective connectivity, it is easier to envisage the singlet "tetrahedral" $[N_2O_2]^{2+}$ complex dissociating directly to $NO_2^{2+} + N$ than the linear triplet complex with its N–N–O–O atomic arrangement. If the reaction conserves spin and proceeds via the singlet "tetrahedral" complex this would implicate the $c(^3\Sigma_u^+)$ state of N_2^{2+} as the reactant. However, spin-flipping

processes in dicationic dissociations are known [151] and the exothermicity spectrum certainly hints strongly that the ground state of the dication is also involved in the reaction. Of course, it is perfectly possible that both electronic states of the dication react with O_2.

In summary, the PSCO spectra clearly indicate that the formation of $NO^+ + O^+ + N$ from collisions of $N_2{}^{2+}$ with O_2 proceeds via the formation of a collision complex which then dissociates, via neutral loss, to leave an $NO_2{}^{2+}$ dication. This dication then decays to $NO^+ + O^+$. Quantum chemical investigations support this idea of local minima, corresponding to collision complexes, existing on the $[N_2O_2]^{2+}$ potential energy surface.

3.2.2. Formation of $NO^+ + N^+ + O$

The scattering diagrams extracted from the PSCO data for this channel [148] look exceptionally similar to those presented for the formation of $NO^+ + O^+ + N$. The scattering diagrams show again that the products NO^+, N^+ and O are isotropically scattered in the CM frame. Again, this isotropic scattering is strong indication that the products have been formed from the break-up of a collision complex which is sufficiently long-lived to rotate before dissociation. Analogously to reaction (35), the data shows that there is a strong anti-correlation between the velocities of the charged products, NO^+ and N^+, whilst the velocity of the neutral fragment, O in this case, is not correlated with either of the charged products.

Hence, similarly to the reaction forming NO^+, N^+ and O, the data strongly indicates that the mechanism for the formation of $NO^+ + N^+ + O$ is

$$N_2{}^{2+} + O_2 \rightarrow [N_2O_2]^{2+} \rightarrow [N_2O]^{2+} + O \rightarrow NO^+ + N^+ + O \quad (38)$$

Again, the N_2O^{2+} dication is well known to possess long-lived metastable states which could readily survive for several hundred picoseconds before dissociating to $NO^+ + N^+$ [47,152].

Using the *ab initio* geometries of the $[N_2O_2]^{2+}$collision complex we estimate [153] that the rotational period for both these complexes, given the considerable angular momentum of our collision system, to be of the order of 20 fs, indicating that the $[N_2O_2]^{2+}$ collision complex must survive for approximately 100 fs before dissociating. This analysis emphasizes that these dicationic collision complexes do not have to live for hundreds of picoseconds for their decay to exhibit scattering indicative of complexation, as due to the high angular momentum of these collision systems the complexes possess very short rotational periods.

3.2.3. Other reactions of $N_2{}^{2+}$

Investigations of the reactions of $N_2{}^{2+}$ with other small molecules, of relevance in the ionospheric chemistry of various planets, reveal a rich range of reactivity. For example with C_2H_2, encounters of relevance to the ionosphere of Titan, we observe the following bond-forming reactions:

$$N_2{}^{2+} + C_2H_2 \rightarrow H^+ + NC_2{}^+ + NH \quad (39)$$

$$N_2{}^{2+} + C_2H_2 \rightarrow H^+ + NC_2H^+ + N \quad (40)$$

$$N_2{}^{2+} + C_2H_2 \rightarrow N^+ + NC_2{}^+ + H_2 \quad (41)$$

$$N_2{}^{2+} + C_2H_2 \rightarrow N^+ + NC_2H^+ + H \quad (42)$$

Whist with H_2O we observe a variety of reactions forming NO^+:

$$N_2{}^{2+} + H_2O \rightarrow NO^+ + NH^+ + H \quad (43)$$

$$N_2{}^{2+} + H_2O \rightarrow NO^+ + H_2{}^+ + N \quad (44)$$

$$N_2{}^{2+} + H_2O \rightarrow NO^+ + H^+ + NH \quad (45)$$

$$N_2{}^{2+} + H_2O \rightarrow NO^+ + N^+ + 2H \quad (46)$$

NO^+ formation is also observed following collisions between $N_2{}^{2+}$ and CO_2, although this reaction is much weaker than the electron-transfer reactivity observed in this collision system:

$$N_2{}^{2+} + CO_2 \rightarrow CO^+ + NO^+ + N \quad (47)$$

The detailed extraction and analysis of the dynamics of these chemical processes from the PSCO data is in progress.

The sensitivity of the PSCO experiment is demonstrated by the observation of a new, but weak, bond-forming reactions. For example, following collisions of $N_2{}^{2+}$ with Ar, the PSCO spectrum shows clear but low intensity signals corresponding to the formation of $ArN^+ + N^+$:

$$N_2{}^{2+} + Ar \rightarrow ArN^+ + N^+ \quad (48)$$

Bond-forming reactivity of molecular dications with the rare gases has been reported before, where channels forming dicationic products have been observed, as well as channels forming pairs of monocations [115,129]. This PSCO observation provides the first opportunity to probe the dynamics of this class of reactions. The exothermicity spectrum we extract for this reaction reveals the dominant energy difference between the reactants and products lies between 2 and 8 eV, peaking at 6 eV. This exothermicity distribution correlates well with the reaction of ground state reactants to give ground state products, for which we calculate an expected exothermicity of 6.3 eV:

$$N_2{}^{2+}(X^1\Sigma_g{}^+) + Ar(^1S_0) \rightarrow ArN^+(^3\Sigma^-) + N^+(^3P) \quad (49)$$

However, the range of observed exothermicities also encompasses the reaction of the $c(^3\Sigma_u{}^+)$ excited state of $N_2{}^{2+}$ to form the $2p^2$ singlet states of N^+ and the ground electronic state of ArN^+. However, it seems clear the products are formed in their ground electronic configurations.

The angular scattering extracted from the weak coincidence signals for this reaction, illustrated in Fig. 17, clearly shows the products are distributed over a wide range of scattering angles, particularly in comparison with a typical dicationic electron-transfer reaction (Fig. 5) [134], indicating the involvement of an encounter complex in the reaction mechanism. It is important to realize in the interpretation of the scattering diagrams derived from the PSCO data, such as Fig. 17, that the PSCO experiment captures the total angular scattering. Thus, the scattering diagrams showing intensity as a function of scattering angle φ, are an integration over the azimuthal angle with respect to v_c and will show a different intensity distribution to a section

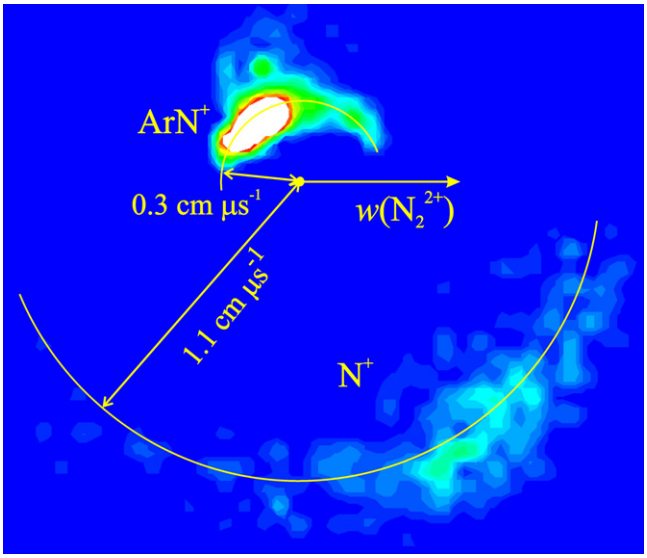

Fig. 17. Scattering diagram showing the velocities of the product ions, N^+ and ArN^+ from reaction (48), relative to the velocity of the N_2^{2+} reactant at 7.1 eV in the CM frame. The data for the ArN^+ product ions are displayed in the upper semicircle of the figure and the data for the N^+ ions are displayed in the lower semicircle of the figure.

in φ at fixed azimuthal angle. Hence, the angular maxima in Fig. 17 are displaced from $\varphi = 0°$. Despite this integration over the azimuthal angle, which emphasizes values of φ close to 90°, it is clear from Fig. 17 that the products are scattered over a wide range of angles without showing the totally symmetrical scattering expected if a collision complex lives for much longer than its rotational lifetime. Thus, this reaction seems to proceed via an "encounter complex" which lives on average for less than its rotational lifetime.

Computational geometry optimizations with a cc-VTZ basis set, using both MP2 and B3LYP methodologies indicate that linear and C_{2v} minima exist on the singlet and triplet ArN_2^{2+} surfaces [154]. The geometries of these complexes derived by the MP2 algorithm, which are very similar those derived by the B3LYP methodology, are detailed in Table 1. The singlet ArN_2^{2+} minima lies, according to CCSD(T) calculations, 7.8 eV below the ground state reactant asymptote, whilst the triplet minimum lies 1.5 eV below the reaction asymptote for the $c(^3\Sigma_u^+)$ state of N_2^{2+}. So collision complexes are definitely energetically accessible to the reactants, in accord with the experimental observations. Given the above observations it seems clear that, as had been postulated earlier, even dicationic bond-forming reactions involving rare gas atoms proceed via collision complexes [132].

Table 1
Calculated geometries of singlet and triplet minima of ArN_2^{2+} geometries

Multiplicity	Symmetry	r(Ar–N) (Å)	r(N–N) (Å)
1	$C_{\infty v}$	1.64	1.14
3	C_{2v}	1.96	1.35

See text for details of the calculations.

4. Conclusions

Position-sensitive coincidence spectroscopy is proving a powerful probe of the reactivity and reaction dynamics of small molecular dications with neutral molecules. The spectra show that the bond-forming reactions of molecular dications often proceed via the formation of a collision complex, although direct reaction pathways have also been observed. For reactions involving a collision complex, these intermediates initially decay towards the observed products by either charge-separation or neutral loss.

Acknowledgements

The experimental work, and its interpretation, presented in this paper would not have been possible without the great efforts of the current and former members of the "Ion Chemistry" research group at UCL; in particular, Sunny Hu, Sarah Harper and Claire Rickets who have helped develop the PSCO experiment. Thanks are also due to Paul Burnside and Simon King for their work on other aspects of dication chemistry which have been touched upon in this article. Nik Kaltsoyannis and Natalie Lambert are also acknowledged for their significant contribution to the computational study of the potential energy surfaces of dication–neutral systems. Thanks are also due to the all the members of the EU "MCInet" Network, in particular Detlef Schröder, Davide Bassi, Tilmann Märk, Jan Hrušák, Hanspeter Winter and Zdenek Herman, for their interest in, and critical comments on, the PSCO results. Odile Dutuit and Roland Thissen are also gratefully acknowledged for stimulating the PSCO experiments involving N_2^{2+} by circulating their unpublished mass spectra showing the products of the $N_2^{2+} + O_2$ reaction. These experiments would not have been possible without the financial support of the EPSRC, the Leverhulme Trust, UCL and the EU.

References

[1] D. Schroder, H. Schwarz, J. Phys. Chem. A 103 (1999) 7385.
[2] D. Mathur, Phys. Rep. 391 (2004) 1.
[3] Z. Herman, Int. Rev. Phys. Chem. 15 (1996) 299.
[4] S.D. Price, Phys. Chem. Chem. Phys. 5 (2003) 1717.
[5] S.G. Cox, A.D.J. Critchley, P.S. Kreynin, I.R. McNab, R.C. Shiell, F.E. Smith, Phys. Chem. Chem. Phys. 5 (2003) 663.
[6] R.B. Metz, Int. J. Mass Spectrom. 235 (2004) 131.
[7] J. Jasik, J. Roithova, J. Zabka, A. Pysanenko, L. Feketeova, I. Ipolyi, T.D. Mark, Z. Herman, Int. J. Mass Spectrom. 249 (2006) 162.
[8] D. Schroder, H. Schwarz, J.L. Wu, C. Wesdemiotis, Chem. Phys. Lett. 343 (2001) 258.
[9] N.R. Walker, G.A. Grieves, J.B. Jaeger, R.S. Walters, M.A. Duncan, Int. J. Mass Spectrom. 228 (2003) 285.
[10] A.J. Stace, J. Phys. Chem. A 106 (2002) 7993.
[11] D.A. Card, E.S. Wisniewski, D.E. Folmer, A.W. Castleman, J. Chem. Phys. 116 (2002) 3554.
[12] O. Echt, P. Scheier, T.D. Mark, C. R. Phys. 3 (2002) 353.
[13] V.G. Nenajdenko, N.E. Shevchenko, E.S. Balenkova, I.V. Alabugin, Chem. Rev. 103 (2003) 229.
[14] L. Avaldi, A. Huetz, J. Phys. B 38 (2005) S861.
[15] J.H.D. Eland, J. Electron Spectrosc. Relat. Phenom. 144 (2005) 1145.
[16] G.C. King, L. Avaldi, J. Phys. B 33 (2000) R215.
[17] J.S. Briggs, V. Schmidt, J. Phys. B 33 (2000) R1.
[18] J. Roithova, D. Schroder, J. Am. Chem. Soc. 128 (2006) 4208.

[19] J. Lilensten, O. Witasse, C. Simon, H. Solidi-Lose, O. Dutuit, R. Thissen, C. Alcaraz, Geophys. Res. Lett. 32 (2005) (Art. no. L03203).
[20] C. Simon, J. Lilensten, O. Dutuit, R. Thissen, O. Witasse, C. Alcaraz, H. Soldi-Lose, Ann. Geophys. 23 (2005) 781.
[21] O. Witasse, O. Dutuit, J. Lilensten, R. Thissen, J. Zabka, C. Alcaraz, P.L. Blelly, S.W. Bougher, S. Engel, L.H. Andersen, K. Seiersen, Geophys. Res. Lett. 29 (2002) (Art. no. 1263).
[22] J.J. Thompson, Rays of Positive Electricity, Longmans, Green and Co., London, 1921.
[23] R. Conrad, Physik. Z. 31 (1930) 888.
[24] A. Vaughan, Phys. Rev. 38 (1931) 1687.
[25] P.K. Carroll, Can. J. Phys. 36 (1958) 1585.
[26] P.K. Carroll, A.C. Hurley, J. Chem. Phys. 35 (1961) 2247.
[27] M.J. Besnard, L. Hellner, Y. Malinovich, G. Dujardin, J. Chem. Phys. 85 (1986) 1316.
[28] P.C. Cosby, R. Moller, H. Helm, Phys. Rev. A 28 (1983) 766.
[29] T.E. Masters, P.J. Sarre, J. Chem. Soc. Faraday Trans. 86 (1990) 2005.
[30] A.S. Mullin, D.M. Szaflarski, K. Yokoyama, G. Gerber, W.C. Lineberger, J. Chem. Phys. 96 (1992) 3636.
[31] M. Larsson, G. Sundstrom, L. Brostrom, S. Mannervik, J. Chem. Phys. 97 (1992) 1750.
[32] P.A. Martin, F.R. Bennett, J.P. Maier, J. Chem. Phys. 100 (1994) 4766.
[33] R. Abusen, F.R. Bennett, I.R. McNab, D.N. Sharp, R.C. Shiell, C.A. Woodward, J. Chem. Phys. 108 (1998) 1761.
[34] L.G.M. Pettersson, L. Karlsson, M.P. Keane, A.N. Debrito, N. Correia, M. Larsson, L. Brostrom, S. Mannervik, S. Svensson, J. Chem. Phys. 96 (1992) 4884.
[35] F.M. Harris, Int. J. Mass Spectrom. Ion. Proc. 120 (1992) 1.
[36] A.G. Brenton, J. Mass Spectrom. 30 (1995) 657.
[37] H. Schwarz, Pure Appl. Chem. 61 (1989) 685.
[38] T. Weiske, W. Koch, H. Schwarz, J. Am. Chem. Soc. 115 (1993) 6312.
[39] D.M. Curtis, J.H.D. Eland, Int. J. Mass Spectrom. Ion. Proc. 63 (1985) 241.
[40] N. Levasseur, P. Millie, J. Chem. Phys. 92 (1990) 2974.
[41] M. Larsson, P. Baltzer, S. Svensson, B. Wannberg, N. Martensson, A.N. Debrito, N. Correia, M.P. Keane, M. Carlssongothe, L. Karlsson, J. Phys. B 23 (1990) 1175.
[42] J. Senekowitsch, S. Oneil, J. Chem. Phys. 95 (1991) 1847.
[43] D.M. Szaflarski, A.S. Mullin, K. Yokoyama, M.N.R. Ashfold, W.C. Lineberger, J. Phys. Chem. 95 (1991) 2122.
[44] D. Edvardsson, S. Lunell, F. Rakowitz, C.M. Marian, L. Karlsson, Chem. Phys. 229 (1998) 203.
[45] D. Mathur, L.H. Andersen, P. Hvelplund, D. Kella, C.P. Safvan, J. Phys. B 28 (1995) 3415.
[46] L.H. Andersen, J.H. Posthumus, O. Vahtras, H. Agren, N. Elander, A. Nunez, A. Scrinzi, M. Natiello, M. Larsson, Phys. Rev. Lett. 71 (1993) 1812.
[47] T.A. Field, J.H.D. Eland, Chem. Phys. Lett. 211 (1993) 436.
[48] M. Lundqvist, D. Edvardsson, P. Baltzer, B. Wannberg, J. Phys. B 29 (1996) 1489.
[49] D. Edvardsson, M. Lundqvist, P. Baltzer, B. Wannberg, S. Lunell, Chem. Phys. Lett. 256 (1996) 341.
[50] A.D.J. Critchley, G.C. King, P. Kreynin, M.C.A. Lopes, I.R. McNab, A.J. Yencha, Chem. Phys. Lett. 349 (2001) 79.
[51] J.H.D. Eland, Chem. Phys. 294 (2003) 171.
[52] J.H.D. Eland, S.S.W. Ho, H.L. Worthington, Chem. Phys. 290 (2003) 27.
[53] J.H.D. Eland, M. Hochlaf, G.C. King, P.S. Kreynin, R.J. LeRoy, I.R. McNab, J.M. Robbe, J. Phys. B 37 (2004) 3197.
[54] M. Alagia, B.G. Brunetti, P. Candori, S. Falcinelli, M.M. Teixidor, F. Pirani, R. Richter, S. Stranges, F. Vecchiocattivi, J. Chem. Phys. 120 (2004) 6980.
[55] A.J. Yencha, A.M. Juarez, S.P. Lee, G.C. King, F.R. Bennett, F. Kemp, I.R. McNab, Chem. Phys. 303 (2004) 179.
[56] A.J. Yencha, A.M. Juarez, S.P. Lee, G.C. King, Chem. Phys. Lett. 381 (2003) 609.
[57] R.I. Hall, L. Avaldi, G. Dawber, A.G. Mcconkey, M.A. Macdonald, G.C. King, Chem. Phys. 187 (1994) 125.
[58] S. Hsieh, J.H.D. Eland, Int. J. Mass Spectrom. 167 (1997) 415.
[59] S. Hsieh, J.H.D. Eland, J. Phys. B 30 (1997) 4515.
[60] S. Hsieh, J.H.D. Eland, Rapid Commun. Mass Spectrom. 9 (1995) 1261.
[61] B.P. Tsai, J.H.D. Eland, Int. J. Mass Spectrom. Ion. Proc. 36 (1980) 143.
[62] S. Leach, J.H.D. Eland, S.D. Price, J. Phys. Chem. 93 (1989) 7583.
[63] S. Leach, J.H.D. Eland, S.D. Price, J. Phys. Chem. 93 (1989) 7575.
[64] P. Calandra, C.S.S. O'Connor, S.D. Price, J. Chem. Phys. 112 (2000) 10821.
[65] S. Harper, P. Calandra, S.D. Price, Phys. Chem. Chem. Phys. 3 (2001) 741.
[66] J.H.D. Eland, Chem. Phys. 323 (2006) 391.
[67] M. Rabrenovic, C.J. Proctor, T. Ast, C.G. Herbert, A.G. Brenton, J.H. Beynon, J. Phys. Chem. 87 (1983) 3305.
[68] P.E.M. Siegbahn, Chem. Phys. 66 (1982) 443.
[69] T. Ast, C.J. Porter, C.J. Proctor, J.H. Beynon, Chem. Phys. Lett. 78 (1981) 439.
[70] C. Heinemann, D. Schroder, H. Schwarz, J. Phys. Chem. 99 (1995) 16195.
[71] P. Bolognesi, M. Coreno, G. Alberti, R. Richter, R. Sankari, L. Avaldi, J. Electron Spectrosc. Relat. Phenom. 141 (2004) 105.
[72] P. Bolognesi, G.C. King, L. Avaldi, Radiat. Phys. Chem. 70 (2004) 207.
[73] J.H.D. Eland, O. Vieuxmaire, T. Kinugawa, P. Lablanquie, R.I. Hall, F. Penent, Phys. Rev. Lett. 90 (2003) (Art. no. 053003).
[74] R. Feifel, J.H.D. Eland, Phys. Rev. A 73 (2006) (Art. no. 019906).
[75] R. Feifel, J.H.D. Eland, Phys. Rev. A 71 (2005) (Art. no. 034501).
[76] P. Bolognesi, D.B. Thompson, L. Avaldi, M.A. MacDonald, M.C.A. Lopes, D.R. Cooper, G.C. King, Phys. Rev. Lett. 82 (1999) 2075.
[77] S.D. Price, J.H.D. Eland, J. Phys. B 24 (1991) 4379.
[78] N.A. Love, S.D. Price, Phys. Chem. Chem. Phys. 6 (2004) 4558.
[79] B.G. Lindsay, M.A. Mangan, H.C. Straub, R.F. Stebbings, J. Chem. Phys. 112 (2000) 9404.
[80] H.C. Straub, B.G. Lindsay, K.A. Smith, R.F. Stebbings, J. Chem. Phys. 108 (1998) 109.
[81] H.C. Straub, B.G. Lindsay, K.A. Smith, R.F. Stebbings, J. Chem. Phys. 105 (1996) 4015.
[82] R. Basner, M. Gutkin, J. Mahoney, V. Tarnovsky, H. Deutsch, K. Becker, J. Chem. Phys. 123 (2005) (Art. no. 054313).
[83] S. Feil, A. Bacher, M. Zangerl, W. Schustereder, K. Gluch, P. Scheier, Int. J. Mass Spectrom. 233 (2004) 325.
[84] K. Gluch, P. Scheier, W. Schustereder, T. Tepnual, L. Feketeova, C. Mair, S. Matt-Leubner, A. Stamatovic, T.D. Mark, Int. J. Mass Spectrom. 228 (2003) 307.
[85] T.D. Mark, in: T.D. Mark, G.H. Dunn (Eds.), Electron Impact Ionization, Springer-Verlag, New York, 1985, p. 137.
[86] P. Franceschi, R. Thissen, J. Zabka, J. Roithova, Z. Herman, O. Dutuit, Int. J. Mass Spectrom. 228 (2003) 507.
[87] C.J. Reid, J.A. Ballantine, F.M. Harris, Int. J. Mass Spectrom. Ion. Proc. 93 (1989) 23.
[88] C.J. Reid, F.M. Harris, J.H. Beynon, Int. J. Mass Spectrom. Ion. Proc. 82 (1988) 151.
[89] J.M. Curtis, R.K. Boyd, J. Chem. Phys. 80 (1984) 1150.
[90] Z. Herman, P. Jonathan, A.G. Brenton, J.H. Beynon, Chem. Phys. Lett. 141 (1987) 433.
[91] M. Hamdan, A.G. Brenton, J. Phys. B 22 (1989) L45.
[92] J.M. Curtis, A.G. Brenton, J.H. Beynon, R.K. Boyd, Chem. Phys. 117 (1987) 325.
[93] K. Vekey, A.G. Brenton, J.H. Beynon, J. Phys. Chem. 90 (1986) 3569.
[94] D. Mathur, R.G. Kingston, F.M. Harris, J.H. Beynon, J. Phys. B 19 (1986) L575.
[95] V. Krishnamurthi, K. Nagesha, V.R. Marathe, D. Mathur, Phys. Rev. A 44 (1991) 5460.
[96] L.E. Dejarme, R.G. Cooks, T. Ast, Org. Mass Spectrom. 27 (1992) 667.
[97] J.O.K. Pedersen, P. Hvelplund, J. Phys. B 20 (1987) L317.
[98] H.R. Koslowski, H. Lebius, V. Staemmler, R. Fink, K. Wiesemann, B.A. Huber, J. Phys. B 24 (1991) 5023.
[99] S.A. Rogers, S.D. Price, S.R. Leone, J. Chem. Phys. 98 (1993) 280.
[100] S.D. Price, S.A. Rogers, S.R. Leone, J. Chem. Phys. 98 (1993) 9455.
[101] N. Tafadar, N. Kaltsoyannis, S.D. Price, Int. J. Mass Spectrom. 192 (1999) 205.

[102] Y.Y. Lee, S.R. Leone, P.H. Champkin, N. Kaltsoyannis, S.D. Price, J. Chem. Phys. 106 (1997) 7981.
[103] S.D. Price, M. Manning, S.R. Leone, Chem. Phys. Lett. 214 (1993) 553.
[104] M. Manning, S.D. Price, S.R. Leone, J. Chem. Phys. 99 (1993) 8695.
[105] A. Ehbrecht, N. Mustafa, C. Ottinger, Z. Herman, J. Chem. Phys. 105 (1996) 9833.
[106] E.Y. Kamber, K. Akgungor, C.P. Safvan, D. Mathur, Chem. Phys. Lett. 258 (1996) 336.
[107] D. Mathur, R.G. Kingston, F.M. Harris, A.G. Brenton, J.H. Beynon, J. Phys. B 20 (1987) 1811.
[108] S.D. Price, J. Chem. Soc. Faraday Trans. 93 (1997) 2451.
[109] B.K. Chatterjee, R. Johnsen, J. Chem. Phys. 91 (1989) 1378.
[110] R. Tonkyn, J.C. Weisshaar, J. Am. Chem. Soc. 108 (1986) 7128.
[111] L.M. Roth, B.S. Freiser, Mass Spectrom. Rev. 10 (1991) 303.
[112] J.C. Weisshaar, Accounts Chem. Res. 26 (1993) 213.
[113] S.D. Price, M. Manning, S.R. Leone, J. Am. Chem. Soc. 116 (1994) 8673.
[114] N. Lambert, N. Kaltsoyannis, S.D. Price, J. Zabka, Z. Herman, J. Phys. Chem. A 110 (2006) 2898.
[115] P.W. Burnside, S.D. Price, Int. J. Mass Spectrom. 249 (2006) 279.
[116] N. Lambert, D. Kearney, N. Kaltsoyannis, S.D. Price, J. Am. Chem. Soc. 126 (2004) 3658.
[117] D. Kearney, S.D. Price, Phys. Chem. Chem. Phys. 5 (2003) 1575.
[118] N. Lambert, N. Kaltsoyannis, S.D. Price, J. Chem. Phys. 119 (2003) 1421.
[119] N. Tafadar, S.D. Price, Int. J. Mass Spectrom. 223–224 (2003) 547.
[120] N. Tafadar, D. Kearney, S.D. Price, J. Chem. Phys. 115 (2001) 8819.
[121] K.A. Newson, N. Tafadar, S.D. Price, J. Chem. Soc. Faraday Trans. 94 (1998) 2735.
[122] K.A. Newson, S.D. Price, Chem. Phys. Lett. 294 (1998) 223.
[123] K.A. Newson, S.D. Price, Chem. Phys. Lett. 269 (1997) 93.
[124] J. Roithova, J. Zabka, J. Hrusak, R. Thissen, Z. Herman, J. Phys. Chem. A 107 (2003) 7347.
[125] L. Mrazek, J. Zabka, Z. Dolejsek, J. Hrusak, Z. Herman, J. Phys. Chem. A 104 (2000) 7294.
[126] Z. Herman, J. Zabka, Z. Dolejsek, M. Farnik, Int. J. Mass Spectrom. 192 (1999) 191.
[127] Z. Dolejsek, M. Farnik, Z. Herman, Chem. Phys. Lett. 235 (1995) 99.
[128] J. Roithova, R. Thissen, J. Zabka, P. Franceschi, O. Dutuit, Z. Herman, Int. J. Mass Spectrom. 228 (2003) 487.
[129] W.Y. Lu, P. Tosi, D. Bassi, J. Chem. Phys. 112 (2000) 4648.
[130] J. Roithova, Z. Herman, D. Schroder, H. Schwarz, Chem.-A Eur. J. 12 (2006) 2465.
[131] C. Nicolas, C. Alcaraz, R. Thissen, J. Zabka, O. Dutuit, Planet Space Sci. 50 (2002) 877.
[132] D. Ascenzi, P. Franceschi, P. Tosi, D. Bassi, M. Kaczorowska, J.N. Harvey, J. Chem. Phys. 118 (2003) 2159.
[133] P. Lablanquie, J. Electron Spectrosc. Relat. Phenom. 76 (1995)63.
[134] S.M. Harper, W.-P. Hu, S.D. Price, J. Phys. B 35 (2002) 4409.
[135] W.P. Hu, S.M. Harper, S.D. Price, Meas. Sci. Technol. 13 (2002) 1512.
[136] L. Wahlin, Nucl. Instrum. Meth. Phys. Res. Sect. A-Accel. Spectrom. Dect. Assoc. Equip. 27 (1964) 55.
[137] K. Yamasaki, S.R. Leone, J. Chem. Phys. 90 (1989) 964.
[138] J.H.D. Eland, Meas. Sci. Technol. 4 (1993) 1522.
[139] I. Ali, R. Dorner, O. Jagutzki, S. Nuttgens, V. Mergel, L. Spielberger, K. Khayyat, T. Vogt, H. Brauning, K. Ullmann, R. Moshammer, J. Ullrich, S. Hagmann, K.O. Groeneveld, C.L. Cocke, H. Schmidt-Bocking, Nucl. Instrum. Meth. Phys. Res. Sect. B-Beam Interact. Mater. Atoms 149 (1999) 490.
[140] A. Oelsner, O. Schmidt, M. Schicketanz, M. Klais, G. Schonhense, V. Mergel, O. Jagutzki, H. Schmidt-Bocking, Rev. Sci. Inst. 72 (2001) 3968.
[141] S.M. Harper, S.W.P. Hu, S.D. Price, J. Chem. Phys. 120 (2004) 7245.
[142] W.P. Hu, S.M. Harper, S.D. Price, Mol. Phys. 103 (2005) 1809.
[143] B. Friedrich, Z. Herman, Chem. Phys. Lett. 107 (1984) 375.
[144] B. Friedrich, S. Pick, L. Hladek, Z. Herman, E.E. Nikitin, A.I. Reznikov, S.Y. Umanskii, J. Chem. Phys. 84 (1986) 807.
[145] S.M. Harper, S.W.P. Hu, S.D. Price, J. Chem. Phys. 121 (2004) 3507.
[146] A.P. Levick, T.E. Masters, D.J. Rodgers, P.J. Sarre, Q.S. Zhu, Phys. Rev. Lett. 63 (1989) 2216.
[147] D.M. Hirst, M.F. Guest, Mol. Phys. 49 (1983) 1461.
[148] C.L. Ricketts, S.M. Harper, S.W.P. Hu, S.D. Price, J. Chem. Phys. 123 (2005) (Art. no. 134322).
[149] P.G. Fournier, J.H.D. Eland, P. Millie, S. Svensson, S.D. Price, J. Fournier, G. Comtet, B. Wannberg, L. Karlsson, P. Baltzer, A. Kaddouri, U. Gelius, J. Chem. Phys. 89 (1988) 3553.
[150] T. Masuoka, A. Kobayashi, Chem. Phys. 302 (2004) 31.
[151] G. Parlant, J. Senekowitsch, S.V. Oneil, D.R. Yarkony, J. Chem. Phys. 94 (1991) 7208.
[152] S.D. Price, J.H.D. Eland, P.G. Fournier, J. Fournier, P. Millie, J. Chem. Phys. 88 (1988) 1511.
[153] R.D. Levine, R.B. Bernstein, Molecular Reaction Dynamics and Chemical Reactivity, Oxford Univeristy Press, Oxford, 1987.
[154] M.J. Frisch, G.W. Trucks, H.B. Schlegel, G.E. Scuseria, M.A. Robb, J.R. Cheeseman, V.G. Zakrzewski, J.A. Montgomery Jr., R.E. Stratmann, J.C. Burant, S. Dapprich, J.M. Millam, A.D. Daniels, K.N. Kudin, M.C. Strain, O. Farkas, J. Tomasi, V. Barone, M. Cossi, R. Cammi, B. Mennucci, C. Pomelli, C. Adamo, S. Clifford, J. Ochterski, G.A. Petersson, P.Y. Ayala, Q. Cui, K. Morokuma, D.K. Malick, A.D. Rabuck, K. Raghavachari, J.B. Foresman, J. Cioslowski, J.V. Ortiz, A.G. Baboul, B.B. Stefanov, G. Liu, A. Liashenko, P. Piskorz, I. Komaromi, R. Gomperts, R.L. Martin, D.J. Fox, T. Keith, M.A. Al-Laham, C.Y. Peng, A. Nanayakkara, M. Challacombe, P.M.W. Gill, B. Johnson, W. Chen, M.W. Wong, J.L. Andres, C. Gonzalez, M. Head-Gordon, E.S. Replogle, J.A. Pople, Gaussian 98, Revision A.9, Gaussian, Inc., Pittsburgh, PA, 1998.